

1-1-2009

Femtosecond Laser Machining At Submicron And Nano Scale

Alireza. Dalili
Ryerson University

Follow this and additional works at: <http://digitalcommons.ryerson.ca/dissertations>

 Part of the [Mechanical Engineering Commons](#)

Recommended Citation

Dalili, Alireza., "Femtosecond Laser Machining At Submicron And Nano Scale" (2009). *Theses and dissertations*. Paper 1083.

This Thesis is brought to you for free and open access by Digital Commons @ Ryerson. It has been accepted for inclusion in Theses and dissertations by an authorized administrator of Digital Commons @ Ryerson. For more information, please contact bcameron@ryerson.ca.

TA
1715
.J88
2009

FEMTOSECOND LASER MACHINING AT SUBMICRON AND NANO SCALE

By

Alireza Dalili

Bachelor of Applied Science

University of Toronto, 2005

A Thesis

presented to

Ryerson University

In partial fulfillment of the requirement for the degree of

Master of Applied Science

in

The Program of Mechanical Engineering

Toronto, Ontario, Canada

Alireza Dalili © 2009

AUTHOR'S DECLARATION

I hereby declare that I am the sole author of this thesis report.

I authorize Ryerson University to lend this thesis to other institutions or individuals for the purpose of scholarly research.

Alireza Dalili
Department of Mechanical and Industrial Engineering
Ryerson University

I further authorize Ryerson University to reproduce this project by photocopying or by other means, in total or in part, at the request of other institutions or individuals for the purpose of scholarly research.

Alireza Dalili
Department of Mechanical and Industrial Engineering
Ryerson University

Femtosecond Laser Machining at Submicron and Nano Scale

Alireza Dalili, Master of Applied Science, 2009

Department of Mechanical and Industrial Engineering, Ryerson University

Abstract

The arrival of the femtosecond laser with a MHz repetition rate has provided the industry with a new tool to conduct submicron and nano scale machining. Several advantages such as high quality machining finish, good precision and high throughput can be obtained when using femtosecond laser to conduct nanomachining over lithography techniques currently in use. High repetition rate systems are preferred over low repetition rate femtosecond laser systems that have been studied by others due to their increased stability, speed, quality and discovery of new phenomena such as ripples and grains.

This thesis proposes a high repetition rate fiber femtosecond laser system for meeting the above-mentioned conditions. The influence of the laser repetition rate and pulse energy on the size and quality of nano features fabricated on silicon wafers was investigated. Higher repetition rates led to smaller cutlines with uniform width. A 110 nm crater with a small heat affected zone of 0.79 μm was obtained at 13 MHz repetition rate and 2.042 J/cm^2 energy fluence. In terms of nanomachining below the ablation threshold (surface patterning), the influence of pulse width, repetition rate and pulse energy on the spacing of ripples, as well as diameter of grains created on silicon wafers, was examined. For the pulsewidth, repetition rate and pulse energy range used, the ripple spacing and grain diameter increased with laser pulse duration while other parameters did not play a significant role. These results show the capability of the proposed system in meeting the industry requirements.

Acknowledgments

I would like to thank my research supervisors, Dr. K. Venkatakrishnan and Dr. Bo Tan, for their outstanding supervision and guidance. Their unconditional support, advice and constructive criticism throughout my research study have been invaluable.

I would like to thank Dr. Greg Kawall, Director of Mechanical Engineering Graduate program, all the faculty members, technical officers and administrative staff members for their kind support and cooperation all the time during my stay at Ryerson University.

I am also grateful to my family for their continued support, prayers and love. Deepest gratitude to my parents, who had to sacrifice their time and needs to support me to finish my studies successfully.

Finally, I am grateful to the Grace of God for the countless blessings I have received.

Table of Contents

Author's Declaration	ii
Abstract	iii
Acknowledgments	iv
Table of Contents	v
List of Figures	vii
List of Tables	x
Nomenclature	xi
Chapter 1: Introduction	1
1.1 Introduction To Nano Fabrication Techniques.....	1
1.2 Research Objectives	11
1.3 Overview of Thesis.....	12
Chapter 2: Laser Ablation Mechanism	13
2.1 Introduction	13
2.2 Nanosecond Laser Ablation.....	15
2.3 Femtosecond Laser Ablation	21
Chapter 3: Experimental Setup	26
3.1 Introduction	26
3.2 Experimental Setup.....	26
Chapter 4: Effect of Repetition Rate	30
4.1 Introduction	30
4.2 Heat Conduction at High Pulse Repetition Rate	32
4.3 Results and Discussion	36
4.3.1 Effects of Laser Fluence Change on Crater Width and Heat Affected Zone	36
4.3.2 Effects of Pulse Repetition Rate on Ablation Threshold	38
4.3.3 Effects of Pulse Repetition Rate on Crater Width and Heat Affected Zone	40
4.4 Summary.....	48

Chapter 5: Silicon Wafer Surface Patterning Using Femtosecond Laser Irradiation Below Ablation Threshold	49
5.1 Introduction	49
5.2 Results and Discussion	52
5.2.1 Ripples.....	52
5.2.1.1 Ripple Formation Mechanisms	52
5.2.1.1.1. Acoustic Wave	52
5.2.1.1.2. Surface Tension Gradients	52
5.2.1.1.3. Interference Between The Incident Light and The Surface Wave .	55
5.2.1.1.4. Boson Condensation Hypothesis.....	57
5.2.1.2 Effect of Pulse Width on Ripple Spacing.....	58
5.2.1.3 Effect of Pulse Energy on Ripple Spacing	63
5.2.2 Grains	64
5.2.2.1 Grain Formation Mechanism	64
5.2.2.2 Effect of Pulse Energy on Grain Diameter.....	64
5.2.2.3 Effect of Pulse Width on Grain Diameter	65
5.3 Summary.....	68
Chapter 6: Summary, Conclusions and Future Work	69
6.1 Summary & Conclusions.....	69
6.2 Future Work.....	71
References	73

List of Figures

Figure 1-1: Optical arrangement for the preparation of regular patterns with sub-half-wavelength resolution using vacuum UV interference lithography with an immersion liquid [1].....	2
Figure 1-2: Comparison of the principle possibilities for nanostructure generation by X-ray lithography (left) and diffraction-limited UV-lithography in multilayer resist technology (right) [1].....	4
Figure 1-3: Principle of an arrangement for EUV exposure using a scanning system and a reflective optical system for pattern transfer [1].....	4
Figure 1-4: Proximity effect by formation of an excitation volume in electron beam lithography [1].....	7
Figure 1-5: Minimization of the proximity effect by heavy elements in the target material or by freestanding membranes [1].....	7
Figure 1-6: Ion Beam System [2].....	9
Figure 2-1: Long-Pulse Laser-Matter Interaction [19].....	15
Figure 2-2: Long-Pulse Avalanche Ionization [19].....	19
Figure 2-3: Creating Sub-Micron Features [19].....	21
Figure 2-4: Short-Pulse Avalanche Ionization [19].....	23
Figure 2-5: Avalanche Ionization [19].....	23
Figure 2-6: Ultrafast Pulse Laser-Matter Interaction [19].....	24
Figure 3-1: Experimental Setup.....	29
Figure 4-1: All images at 13 MHz laser repetition rate. (a) SEM image of 3.340 J/cm ² fluence (b) SEM image of 2.672 J/cm ² fluence (c) SEM image of 2.042 J/cm ² fluence.....	37
Figure 4-2: Threshold Energy Fluence vs. Repetition Rate from 1 MHz to 13 MHz.....	39

Figure 4-3: Threshold Average Beam Power vs. Repetition Rate from 1 MHz to 13 MHz.....	40
Figure 4-4: All images at fluence of 2.917 J/cm ² . (a) SEM image of 4.33 MHz repetition rate (b) SEM image of 5.20 MHz repetition rate.....	41
Figure 4-5: Crater Width vs. Energy Fluence for 6.50 MHz to 13 MHz laser repetition rate.....	43
Figure 4-6: Heat Affected Zone vs. Energy Fluence for 1 MHz to 13 MHz laser repetition rate.....	45
Figure 4-7: SEM image of 2.822 J/cm ² beam energy fluence and 6.50 MHz laser repetition rate cutline with crater width of 220 nm and heat affected zone of 1.25 μm.....	46
Figure 4-8: SEM image of 2.991 J/cm ² beam energy fluence and 8.67 MHz laser repetition rate cutline with crater width of 180 nm and heat affected zone of 1.11 μm.....	47
Figure 4-9: SEM image of 2.042 J/cm ² beam energy fluence and 13 MHz laser repetition rate cutline with crater width of 110 nm and heat affected zone of 0.79 μm.....	47
Figure 5-1: Scheme of the different morphological phenomena after irradiation of silicon surface with linearly polarized femtosecond laser pulses of typically 100 fs duration [7].....	51
Figure 5-2: A midpoint cross section parallel to the laser beam path of a laser-melted surface illustrating rippling and key-holing effects. (a) Just after initiation of the laser beam sweep; (b) rippling and keyholing in steady state; (c) at the conclusion of the laser beam sweep [44].....	54
Figure 5-3: SEM image of ripple formation at 300 fs, 8.67 MHz laser repetition rate and 0.230 W laser power (equivalent to 2.653E-08 J pulse energy).....	59
Figure 5-4: SEM image of ripple formation at 700 fs, 8.67 MHz laser repetition rate and 0.270 W laser power (equivalent to 3.114E-08 J pulse energy).....	60

Figure 5-5: Ripple Spacing vs. Pulse Energy for Pulse Width 300 fs to 5 ps and Repetition Rate of 8.67 and 13 MHz.....63

Figure 5-6: Grain Diameter vs. Pulse Energy for Pulse Width 300 fs to 5 ps and Repetition Rate of 8.67 and 13 MHz.....65

Figure 5-7: Grain Diameter vs. Pulse Width for Laser Repetition Rate of 8.67 and 13 MHz.....66

Figure 5-8: SEM image of grain formation at 700 fs, 13 MHz laser repetition rate and 0.320 W laser power (equivalent to 2.462E-08 J pulse energy).....67

Figure 5-9: SEM image of grain formation at 2000 fs, 8.67 MHz laser repetition rate and 0.249 W laser power (equivalent to 2.872E-08 J pulse energy).....67

List of Tables

Table 1-1: Current and Emerging Nanofabrication Techniques [1].....	2
Table 5-1: Ripple Spacing vs. Pulse Width for Laser Repetition Rate of 8.67 and 13 MHz..	58

Nomenclature

ns	nanosecond (10^{-9} s)
ps	picosecond (10^{-12} s)
fs	femtosecond (10^{-15} s)
μm	micrometer (10^{-6} m)
nm	nanometer (10^{-9} m)
MHz	megahertz (10^6 Hz)
W	watt
GW	gigawatt
μJ	micro-Joule (10^{-6} J)
I_α	absorbed laser intensity
t	time
$2\omega_0$	spot diameter
λ_0	wavelength of the laser beam
f_l	effective focal length of the scan lens
D	diameter of the laser beam at the input of the piezo-scanner
N_{eff}	number of effective pulses at a given spot
f	repetition rate
v	piezo scanning speed
D	feature size
Φ_0	maximum laser fluence
Φ_{TH}	threshold laser fluence
E_{pulse}	laser pulse energy
τ	pulsewidth
E_0	pulse energy
E_{th}	threshold pulse energy
a	thermal diffusion coefficient
k	heat conduction coefficient
C_p	specific heat
t_p	laser pulse duration
t_{pp}	laser repetition rate

T_m	maximum surface temperature
γ	surface tension
ρ	specific gravity
h	ripple base width
V_c	critical laser beam sweep velocity
τ	time required to form ripples
g	acceleration field
σ	surface tension
σ_0	surface enthalpy
S	surface entropy
T	temperature
$d\sigma/dT$	temperature coefficient of the surface tension
ϵ_r	relative permittivity
θ	angle of incidence
Λ	ripple spatial period
d	full width of laser spot size
v_R	Rayleigh velocity
2τ	laser pulse width
k_R	wave vector of the surface acoustic wave
k_l	wave vectors for longitudinal waves
k_t	wave vectors for transverse waves
ϕ and ψ	potentials of the surface acoustic wave

CHAPTER 1

INTRODUCTION

1.1 INTRODUCTION TO NANO FABRICATION TECHNIQUES

According to [1], micro and nano technology has immense impact on our daily lives due to our dependence on computers. The size of typical micro structures that is accessible is in the sub-micrometer range, which is at the limits of optical resolution and barely visible with a light microscope. This is about 1/1000 smaller than structures resolvable by the naked eye, but still 1000 times larger than an atom. Today's developments are addressing the size range below these dimensions. For instance, nanometric structures are in the 10^{-9} meter range. Because a typical structure size is in the nanometer range, the methods and techniques are defined as nanotechnology. In the following table, Table 1-1, nanofabrication techniques currently in use such as DUV and Vacuum-UV Lithography, EUV and X-ray Lithography, Electron Beam Lithography, Ion Beam Lithography are described. The emerging Femtosecond Laser Nanomachining method is touched upon and will be described fully in Chapter 2. Table 1-1 is a rephrased, summarized and tabular version of similar sections in [1].

Technique	Description	Advantages	Disadvantages
<p align="center">DUV and Vacuum-UV Lithography</p>	<ul style="list-style-type: none"> • Exposure Area: DUV 250 nm, Vac-UV 90 nm • Large complexes of structures transferred in the size of a chip • Requires High Optical Precision, Homogenous Illumination & Sensitive and Transparent Resists • Improve Resolution by Polarized Light, High Numerical Apertures, Immersion in Liquid & Use of chemically amplification UV resists 	<ul style="list-style-type: none"> • Cost-Efficient & Highly Productive compared to other lithography techniques, but not femtosecond laser nanomachining 	<ul style="list-style-type: none"> • Light Diffraction Issues • Multi-Million Dollar Equipment & Mask • No Rapid Prototyping since slow and expensive • Multistep

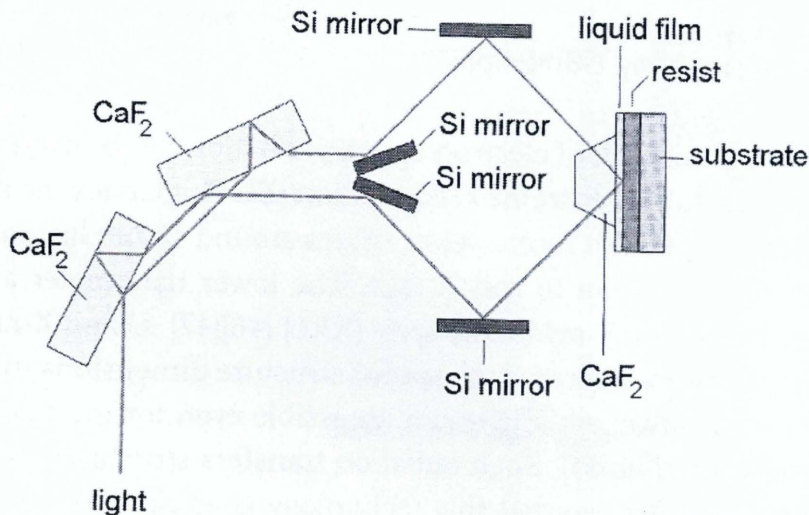


Figure 1-1: Optical arrangement for the preparation of regular patterns with sub-half-wavelength resolution using vacuum UV interference lithography with an immersion liquid [1]

Technique	Description	Advantages	Disadvantages
<p>EUV and X-ray Lithography (XRL)</p>	<ul style="list-style-type: none"> • EUV useful for Medium Nanometric Devices (20-50 nm) 2009 Goal: 32 nm for LSI circuits • XRL for lower Nanometer and Sub-Nanometer range • EUV based on reflection optics • Parallel XRL (PXL) suited for 1:1 pattern transfer and consists of a 10 or 5 μm gap between masks to create 100 or 25 nm level structure • X-ray can be used for direct writing into X-ray sensitive resist 	<ul style="list-style-type: none"> • No Light Diffraction Issues compared to other lithography techniques 	<ul style="list-style-type: none"> • Materials differ in optical transmission • Multi-Million Dollar Equipment & Mask • No Rapid Prototyping since slow and expensive • High Resolution Optics difficult to fabricate • Multistep

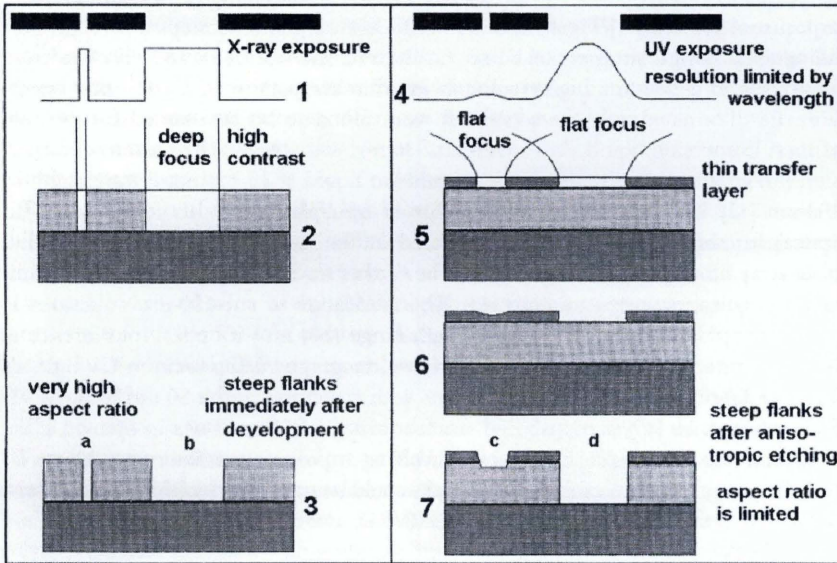


Figure 1-2: Comparison of the principle possibilities for nanostructure generation by X-ray lithography (left) and diffraction-limited UV-lithography in multilayer resist technology (right) [1]

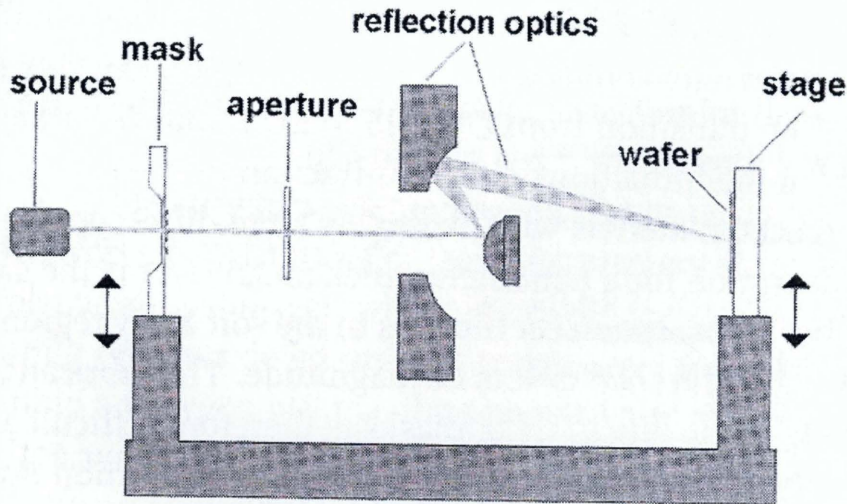


Figure 1-3: Principle of an arrangement for EUV exposure using a scanning system and a reflective optical system for pattern transfer [1]

Technique	Description	Advantages	Disadvantages
<p>Electron Beam Lithography</p>	<ul style="list-style-type: none"> • Sub 10-nm level structures have been realized • Beam divergence by both electric and magnetic (Lorentz effect) fields suppressed by using high acceleration voltage, low beam current & proximity focusing • Fast electrons applied to knock electrons out of inner shells leading to material ionization • Secondary processes broaden the area and depend on atomic number of target • Resolution limited by excitation pear which is caused by proximity effect (0.5- 1 μm for low atomic number elements) • Excitation pear dependent on target material and beam parameters especially acceleration voltage 	<ul style="list-style-type: none"> • Higher resolution than other methods stated • Maskless 	<ul style="list-style-type: none"> • Influenced by Environment • Proximity Effect • Slow Speed • Low Energy so mask fabrication not machining • Multi-Million Dollar Equipment • No Rapid Prototyping since slow and expensive

Technique	Description	Advantages	Disadvantages
<p align="center">Electron Beam Lithography (Continued)</p>	<ul style="list-style-type: none"> • Elements with fewer electrons are easier to ionize so larger penetration depth and less beam diversion • To reduce proximity effect correct local electron dosage used as well as work at the neck of excitation pear • Application in generation of photolithography masks 		

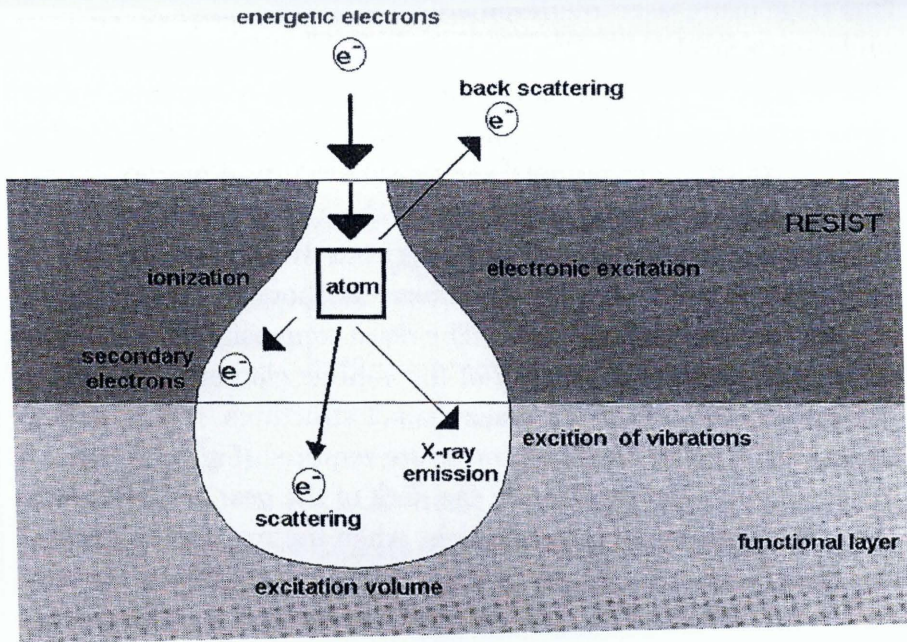


Figure 1-4: Proximity effect by formation of an excitation volume in electron beam lithography [1]

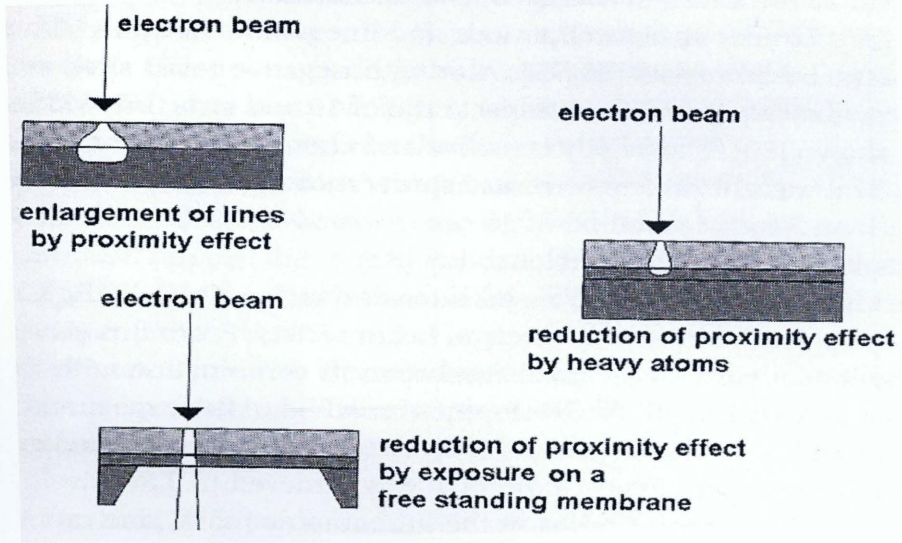


Figure 1-5: Minimization of the proximity effect by heavy elements in the target material or by freestanding membranes [1]

Technique	Description	Advantages	Disadvantages
Ion Beam Lithography	<ul style="list-style-type: none"> • 2-3 nm width cuts in GaAs with Focused Ion Beam (FIB) achieved • 10 nm opening in gold films using combined EBL and FIB • Similar to electron beam lithography except ions used • Ions generated and accelerated by electrodes and guided by electronic optics • Proximity lithography by parallel ion beams with small distance between mask and substrate • High resolution requires constant distance and greater apertures • Ion Beam Lithographic Systems contain vacuum container with ion source, ion optical system, alignment system and table for mask and substrate 	<ul style="list-style-type: none"> • High Resolution • Optical Projection • Higher Productivity than EBL 	<ul style="list-style-type: none"> • Vacuum environment required • Slow Speed • Influenced by Environment • Proximity Effect still present • Multi-Million Dollar Equipment • No Rapid Prototyping since slow and expensive • Mask Fabrication not machining

Technique	Description	Advantages	Disadvantages
<p style="text-align: center;">Ion Beam Lithography (Continued)</p>	<ul style="list-style-type: none"> • FIB favoured over electron beams since less secondary effect and therefore reduced excitation pear and proximity effect • Applications include structures in sensitive resists, local implementation, structure transfer by etching and direct local etching 		

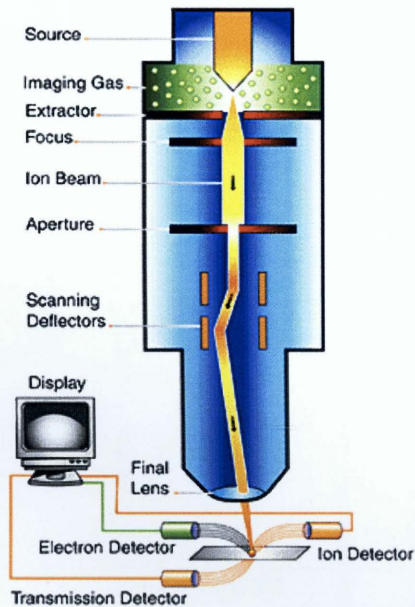


Figure 1-6: Ion Beam System [2]

Technique	Description	Advantages	Disadvantages
<p style="text-align: center;">Femtosecond Laser Nanomachining</p>	<ul style="list-style-type: none"> • Direct solid to vapour transition • Use high peak power of ultrafast laser to create free electrons (saturated Avalanche Effect) and induce multiphoton absorption • Plume (Ion) and electron expansion cause negligible debris • Application in biomedical, microelectronics, photonics and MEMS industries • With new techniques in fiber amplification, high power femtosecond lasers are now available on the market. • Therefore, using a femtosecond laser for nanomachining could be considered a feasible and promising industrial tool. This research was carried out using such a laser system. 	<ul style="list-style-type: none"> • Short Pulse Width – Multiphoton Ionization and absence of energy transfer from electrons to lattice - Minimal Heat Diffusion (Small HAZ) - High Quality Machining Finish • Accurately Controlled Laser Ablation Threshold – Small Laser Spot Size (1/20 wavelength) - Good Machining Precision • Short Pulse Width - High peak intensity with Low Pulse Energy - Highly Efficient Machining (0.01 to 1 $\mu\text{m}/\text{pulse}$) • Atmospheric Conditions • Cheap Equipment • Maskless • Therefore cheaper and less time consuming compared to the lithography techniques mentioned 	<ul style="list-style-type: none"> • Low Average Power leading to Low Throughput. However, new models have average beam power > 20 W leading to high throughput and lowered cost

Table 1-1: Current and Emerging Nanofabrication Techniques [1]

1.2 RESEARCH OBJECTIVES

Even though the feasibility of using femtosecond lasers has been predicted for over a decade now, industrial application of this technique has not been fully realized due to the challenges faced in terms of laser parameters and inadequate experimental studies in this area. The main aim of this thesis is to study the high repetition rate femtosecond laser system and its effect on nanomachining of silicon wafers.

Researchers have been predicting the advantages of using ultra fast laser systems for more than a decade now, but the capabilities of the laser systems used in previous studies did not have the potential of overcoming the throughput and precision requirements in nanomachining. This is true of nanomachining at both below the ablation threshold (surface patterning) and above it (ablation). Laser parameters influencing the size and quality of nano features on silicon wafers are primarily the repetition rate and pulse energy. In terms of surface patterning, laser pulse width is crucial as well. Hence, the outline of the research objectives of this thesis are summarized as follows:

1. Verify the capabilities of the proposed high repetition rate femtosecond laser system for nanomachining of silicon wafers.
2. Evaluate the influence of laser repetition rate and pulse energy on crater width and heat affected zone (HAZ) of silicon wafers during nanomachining above the ablation threshold.
3. Study the influence of the pulse width, repetition rate and pulse energy on the spacing of ripples as well as diameter of grains created on silicon wafers during nanomachining below the ablation threshold (surface patterning).

1.3 OVERVIEW OF THESIS

In Chapter 2, the pulsed laser ablation mechanism is discussed in general. Existing mechanism and theories describing laser-matter interaction during the long pulse and short pulse ablation of silicon are summarized, with special attention to femtosecond laser ablation. Details of the experimental setup are presented in Chapter 3.

A systematic experimental study of the influence of repetition rate using a high repetition rate femtosecond laser for nanoscale material processing is investigated and the results are presented and discussed in Chapter 4. The effect of pulse repetition rate and pulse energy on femtosecond laser machining of gold-coated silicon wafer was studied to determine the optimum values of each of these parameters for processing thin films. Machined lines were analyzed and compared while varying the laser repetition rate from 1 MHz to 13 MHz. At each repetition rate, the average beam power was changed from a value well above the damage threshold down to the point where no machining occurred, namely, below the ablation threshold.

A systematic study of the influence of the pulse width, repetition rate and pulse energy on the spacing of ripples, as well as diameter of grains created during the surface patterning operations, is discussed in Chapter 5. A number of different experiments were performed. The mechanisms and theories leading to the creation of ripples and grains in both the femtosecond and picosecond pulse width ranges were explained.

Chapter 6 summarizes the results obtained from this research work. This chapter also includes suggestions for further research that can be carried out.

CHAPTER 2

LASER ABLATION MECHANISM

2.1 INTRODUCTION

Laser cutting and milling techniques are more accurate than their mechanical counterparts. They are also material independent, which allows for manufacturing of a wide range of products from turbine blades to medical tools [3]. Efficient use of lasers for precise material processing is difficult to understand without thorough knowledge of the fundamental physics governing the interaction of laser radiation with matter [4]. The physical process of laser/matter interaction is indeed very complicated and involves a variety of different phenomena. Much fundamental research has been done to determine the physical mechanisms involved and their relative contributions to the complex and highly non-equilibrium laser/matter interaction process [4-6]. The recent progress in laser systems, specifically the chirped pulse amplification (CPA) technique, has allowed the systematic study of the laser/matter interaction using a broad range of laser parameters [4]. These laser parameters include, but are not limited to, laser fluence, pulse duration, wavelength and laser repetition rate. Thus, the optimal machining conditions can only be achieved by understanding the physical processes in laser/matter interaction, as well as the influence of each of the important laser parameters on these processes. The ablation mechanism is also dependent on the properties of the sample material. Silicon prevails in the semiconductor industry and therefore silicon wafers were used as the laser target in all experiments outlined in this thesis. This chapter focuses on the fundamental physical mechanisms and characteristics of laser/silicon interaction. Laser pulse width plays a crucial role in the ablation mechanism [5-9]. Depending on the pulse width regime, the

mechanism can be thermal or non-thermal in nature. The peak intensity of the laser power can be increased dramatically by shortening the pulse of the laser beam [3]. Picosecond and femtosecond lasers achieve very high peak intensities with low pulse energies. For example, a laser pulse with a width of 100 fs and energy of 0.33 J has a peak intensity of 10^{15} W/cm² when focused onto a 20 μ m spot. A 10-nanosecond long laser pulse would have to be 100 J to reach the same intensity [3]. To better understand the advantages of ablation with femtosecond laser, laser/matter interaction mechanisms are discussed for both femtosecond and nanosecond laser pulse width.

As [10] states, in the micro-manufacturing industry, the laser is being established as an indispensable tool because of the benefits, such as higher etch rates, easier automation and better quality features. Excimer lasers are extensively used for micromachining polymers and ceramics while Nd:YAG lasers are used for microdrilling and marking of semiconductors and metals. However, these lasers (nanosecond to millisecond pulses) are not well suited for precise microstructuring due to thermal or mechanical damages (recast layers, burrs and cracks, etc.), limiting the achievable precision and quality. These shortcomings have spurred the development of ultrafast (pico- and femtosecond) lasers, which deliver enhanced precision and cleanliness of machined features by minimizing collateral damage, plasma effects and thermal diffusion [11–14]. Femtosecond (fs) pulsed lasers are emerging as tools for microfabrication of all types of materials that are used in biomedical, microelectronics, photonics and MEMS industries. The unique characteristics of ultrafast lasers over longer-pulsed lasers are multiphoton ionization and absence of energy transfer from electrons to the lattice, leading to deterministic and reproducible ablation, negligible thermal damage and high etch rates (0.01 to 1 μ m/pulse). These unique advantages make femtosecond lasers promising for the fabrication of a variety of materials such

as low melting point polymers, high thermal conductivity metals, wide bandgap dielectrics and semiconductors that are otherwise difficult to fabricate by conventional tools.

2.2 NANOSECOND LASER ABLATION

Nanosecond laser pulses have been widely used for material removal and micro-fabrication [15-18]. In principle, any type of nanosecond laser with intensities above the ablation threshold could potentially be utilized as the light source for silicon machining (Figure 2-1). There are many nanosecond lasers available, with repetition rates varying from a few 10's of kHz to a few Hz, having a maximum average per pulse intensity from a few GW/cm^2 to up to a thousand GW/cm^2 and pulse lengths from a few nanoseconds to a few tens of nanoseconds. The efficiency of laser pulse utilization in terms of removing material is an important aspect that needs to be known before choosing laser sources.

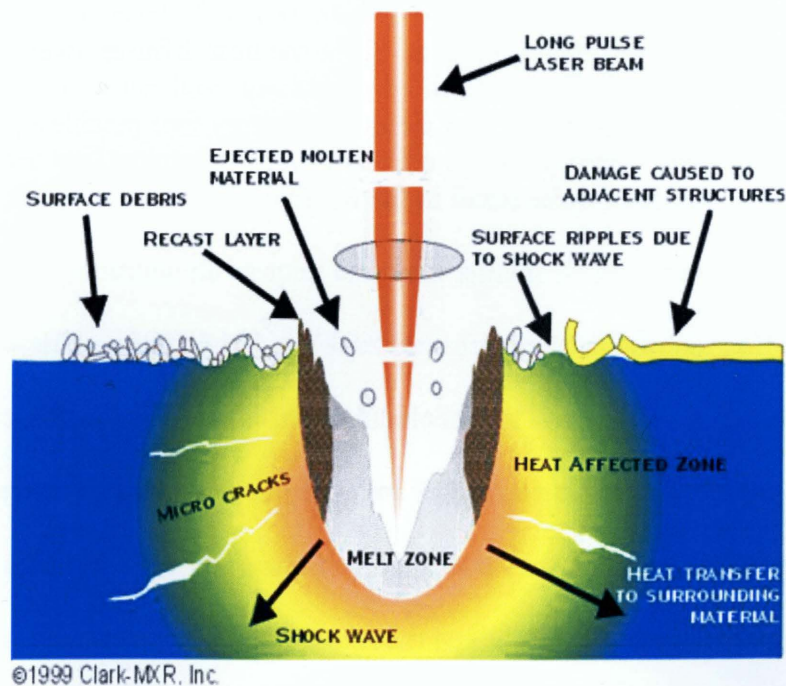


Figure 2-1: Long-Pulse Laser-Matter Interaction [19]

The physical process of laser-silicon interaction in the nanosecond time regime is a complex process, involving many aspects of laser-matter interaction. As [19] states, the most fundamental feature of the interaction in the nano-second regime is heat diffusion into the surrounding material. In other words, the process is thermal in nature involving direct vaporization [20]. There are several reasons why heat diffusion is detrimental to the quality of the nano-machining. First of all, heat diffusion reduces the efficiency of the machining process as it sucks energy away from the work spot. Also, heat diffusion causes the temperature to drop in the focal area which leads to the silicon staying just above the melting point. The silicon is removed through deposition of a lot of energy into it which causes it to boil. The boiling ejects globs of the molten material from the work zone. The ejected globs then form drops which fall back onto the surface and contaminate the sample. The droplets can be quite large and retain a lot of residual heat and will bind strongly to the sample. Removal of these contaminants will be quite hard without damaging the actual silicon sample. Moreover, heat diffusion also decreases the accuracy of the nano-machining process. Since the heat diffuses away from the work spot, an area much larger than the laser spot size melts. Thus, very fine machining cannot be performed. The beam spot size might be quite small in the range of 200 nanometers or less, but it will not be possible to create features much smaller than one micron. In addition, the heat diffusion affects a large area which is referred to “heat-affected zone” or HAZ. The heating and subsequent cooling waves in this region cause a lot of mechanical stress and microcracks (or sometimes macrocracks) which may propagate deeper into the material and cause premature device failure. For instance, the recast layer that forms around the hole is mechanically weaker and has a different structure than the un-melted material. In some devices, such as arterial stent manufacturing, the recast layer is removed through extensive and expensive post-process

cleaning before the device can be used inside the human body. Last but not least, heat diffusion is associated with creation of shockwaves which can damage nearby device structures or delaminate multilayer materials. The more energy deposited into the micromachining process, the stronger the associated shockwaves. With long pulse lasers, the shot to shot reproducibility is poor.

Per [20], in nanosecond lasers, the mechanism involves direct vaporization. The laser beam deposits energy in a shallow layer close to the surface. The surface reaches thermal equilibrium and some of the heat conducts to the material surrounding the laser spot. A molten layer forms and continuous application of the laser vaporizes the substrate. Material is removed by melt expulsion aided by a locally high vapor pressure. The material spatters around the irradiated area and solidifies as residue in the surrounding area. The thermal effects create a thick heat affected zone (HAZ). Shockwaves generated by the explosive change of phase can cause mechanical stress in the material. The formation of liquid and vapor phases around the spot interfere with the precision of the laser machining by deflecting the beam. Laser machining with nanosecond laser pulses lead to a large heat affected area and a large splatter zone for expelled material.

Furthermore, as [19] states, when the laser pulse enters the silicon wafer, the electrons start to oscillate. The sample is made of atoms and electrons. For clarity, Figure 2-2 shows only the electrons. The electrons are either bound or free. Bound electrons are tightly attached to the local atoms. In contrast, free electrons are not tightly attached to the local atoms. The ratio of bound electrons to free electrons is a function of the material. Metals have mostly free electrons, while semiconductors and insulators have very few free electrons. Figure 2-2 shows very few

free electrons. It is representative of a semiconductor. The bound electrons are tightly localized and can only wiggle slightly. In contrast, the free electrons, which are unbound, can oscillate strongly once they are in the laser field. While oscillating, they occasionally collide with the surrounding atoms. If the laser field is intense enough, a free electron colliding with a surrounding atom will knock off an additional electron. Now there are two free electrons that are being driven by the light field. They in turn can knock two more electrons off atoms in the surrounding material. These four electrons create four more free electrons through collisions, and so on. This type of multiplication effect is called an avalanche effect, and, because it creates electrons by ionizing atoms, it is called avalanche ionization. For this avalanche process to start, a free electron must be present initially in the electromagnetic field. The absence of free electrons prevents the avalanche process from significantly starting and ultimately hinders the material ablation. Since in metals there are plenty of free electrons, the avalanche process starts immediately, which leads to reproducible machining. However, there may be other problems associated with heat diffusion. In semiconductors or isolators, there are naturally very few free electrons. The avalanche process may start right away or may not, depending on the presence or absence of a free electron in the beam path. If there are initially several free electrons in the electromagnetic field, then the process will be very efficient. If there are no free electrons, then the process will not start. Therefore, the initiation of the machining process is based on luck. This variability, which is inherent to the physical process, leads to unstable machining rates. Note that the laser may be perfectly stable, the beam spot size and amount of energy in the pulse may be precisely the same from shot-to-shot, yet the material ablation will vary significantly from shot to shot. This is a serious limitation when trying to do very fine machining. If a large quantity of free electrons could be created a priori, then the presence or absence of naturally

occurring free electrons will no longer be an important factor. What matters is the total number of free electrons, not their origin. There are at least two ways to do this. Both approaches rely on the same underlying principle that there are a lot of electrons in the work piece. It is just that the vast majority of them may be bound and not useful to get the avalanche process going. If these bound electrons could be immediately turned into free electrons then the issue would be resolved. This goal can be achieved using lasers working in the ultraviolet or ultrafast regime.

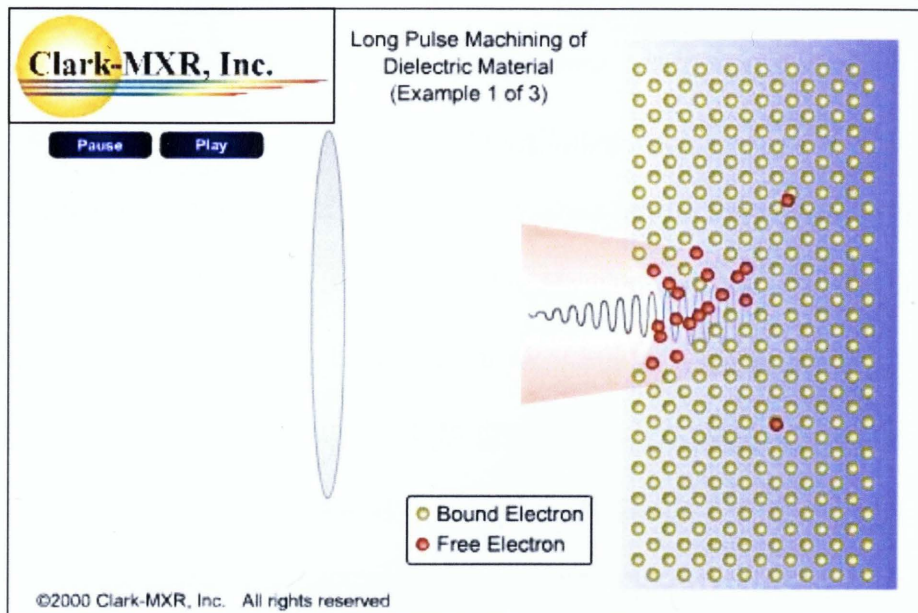


Figure 2-2: Long-Pulse Avalanche Ionization [19]

The unique combination of multiphoton absorption and saturated avalanche ionization provided by ultrafast laser pulses make it possible to machine materials on dimensions smaller than 1 micron [19].

According to [19], in order to create the smallest feature possible by machining with light, the light must be focused on the smallest spot possible. The size of the spot is determined by several factors, but this discussion will be limited to making the statement that the smallest

spot that can be obtained is about the same as the wavelength of the light used to make it. Thus, if the wavelength of light is about 0.5 microns, then the smallest spot will be about 0.5 microns. However, as noted before, while both ultrafast pulse lasers and long pulse lasers can both operate at wavelengths of 0.5 microns, the long pulse laser is not capable of creating a machined feature that is much less than about 10 microns because of heat diffusion into the surrounding material. Referring to Figure 2-3, below, the process by which an ultrafast laser pulse can create features substantially below that of the central wavelength of the laser pulse itself is demonstrated. First, the ultrafast laser is focused on a spot with a profile which has peak intensity in the center of the beam and smoothly decreases radially outward from the center (a "Gaussian" spot). If the intensity of the laser spot on the surface of the material is adjusted so that just the peak of the beam is above threshold, then material will be removed only in that very limited area. That very limited area can be as little as one-tenth the size of the spot itself. Now imagine that ultrafast laser pulses that have a central wavelength of 0.2 microns have been generated. [20] mentions that a feature of ~200 nm in size can be created using a ~600 nm beam. Ultrafast pulses of light can be used to create features as small as 0.02 microns, or 20 nanometers. Without this unique characteristic of machining with ultrafast laser pulses and the highly deterministic nature of the process, it would not be possible to achieve these results without a heat-affected zone. More specifically, it is not possible to get comparable highly repeatable sub-micron machining with long pulse laser systems.

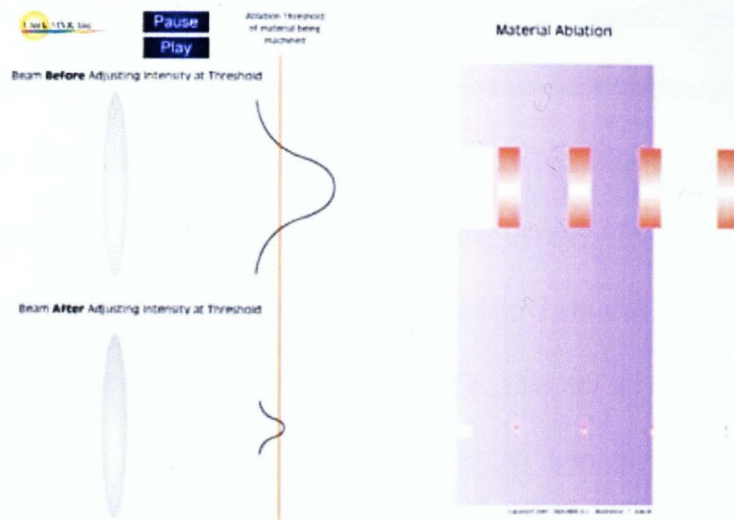


Figure 2-3: Creating Sub-Micron Features [19]

2.3 FEMTOSECOND LASER ABLATION

Femtosecond laser pulses provide an attractive choice as it provides a way to obtain very clean removal of materials. The main advantage of using femtosecond laser pulses for the ablation of materials is that compared with using nanosecond laser pulses, heat diffusion into the target is negligible, which results in much localized ablation and precise patterning of the sample without great thermal damage to the surroundings [4, 5, 19]. The laser pulses illuminate the material for only a short period of time which in turn does not allow the heat deposited into the silicon to move away from the work spot. In other words, the laser pulse duration is shorter than the heat diffusion time. As a result, the laser energy piles up at the working spot leading to increase in the temperature of the silicon past melting and even the evaporation point. It reaches the plasma regime eventually. Furthermore, the peak power delivered by femtosecond lasers is extremely high and easily reaches hundreds of Terawatts per square centimeter range at the work spot. The high power density allows for machining of very hard materials such as Molybdenum

and Rhenium. Moreover, the ultrafast pulse creates the plasma in the surface of the material and the pressures created by the forces within it cause the material to expand outward from the surface in a highly energetic plume or gas. The plume expansion (the expansion of the highly charged atoms “ions”) and electrons from the surface cannot be contained by the internal forces of the material. The electrons which are lighter and more energetic than the ions, come off the material first, followed by the ions. The positively charged ions repel one another as they expand away from the material and as a consequence no debris or droplets condense onto the surrounding material. Since there is no melt phase, there is no splattering of the silicon on the surrounding wafer surface either. One significant difference between femtosecond and nanosecond laser-matter interaction in terms of transferring laser energy into thermal energy of the target is that electrons and ions are not in equilibrium during the laser pulse in the femtosecond laser ablation case. This is because the electron-ion relaxation time, which is in the range of a few picoseconds to a few tens of picoseconds, is much longer than the femtosecond pulse length. Therefore, for the interaction of femtosecond laser pulses with solid materials, the laser energy is first deposited into the thermal energy of electrons and then transferred to the lattice on a picosecond time scale after the laser pulse. As [20] concludes, by the time the laser pulse is turned off, the system is out of equilibrium as the electrons are at a much higher temperature than the ions. In this case, absorption of the laser and heating of the electrons in the surface layer, diffusion of the ‘hot’ electrons into the bulk of the material, as well as the energy exchange between the electron and phonon subsystem, happen simultaneously. The highly concentrated energy causes the material to quickly heat past the melting phase to the vapor phase. Since the heat does not have time to diffuse, the HAZ will be greatly reduced. The depth of the pulse duration determines the thickness of the heated layer and is independent of the pulse

duration. In addition, as [19] mentions, the amplitude of the electromagnetic field corresponds to the peak power of the laser. Ultrafast lasers generate tremendous peak power. As such, the laser pulse can knock free the “bound” electrons in the sample. Therefore, there is a large quantity of free electrons and the avalanche ionization process can start immediately, reliably and reproducibly. This leads to high-quality machining. Figure 2-4 and 2-5 demonstrate this phenomenon.

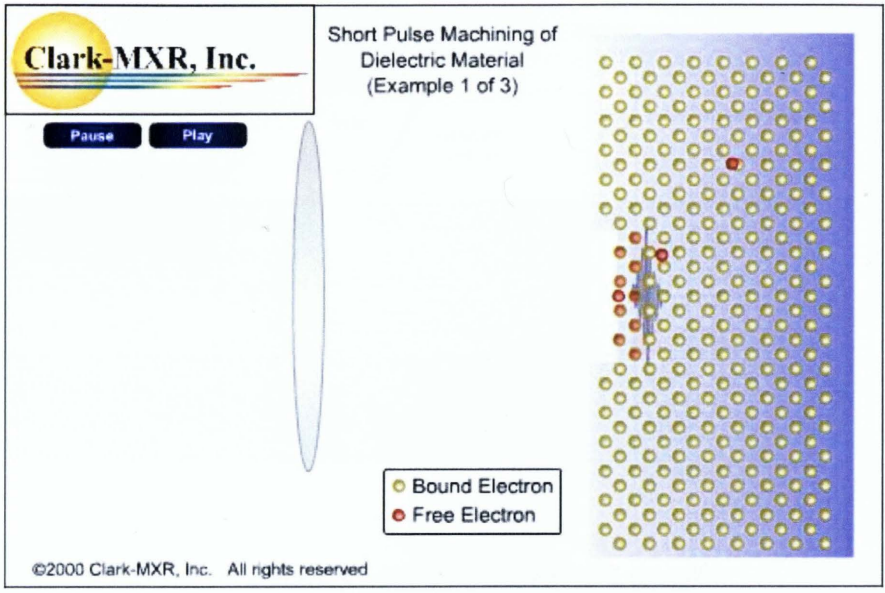


Figure 2-4: Short-Pulse Avalanche Ionization [19]

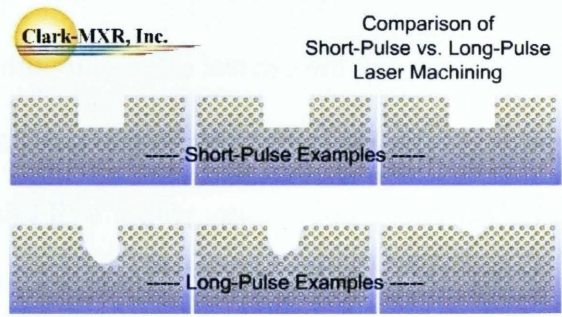


Figure 2-5: Avalanche Ionization [19]

As [20] describes, the ablation is a direct solid-vapor transition. The timescale is to the first order, sufficiently short to ignore all thermal effects and hydrodynamic motion. The minimal HAZ is proof of this phenomenon. Again, this leads to a clean cut with no visible collateral damage (Figure 2-6).

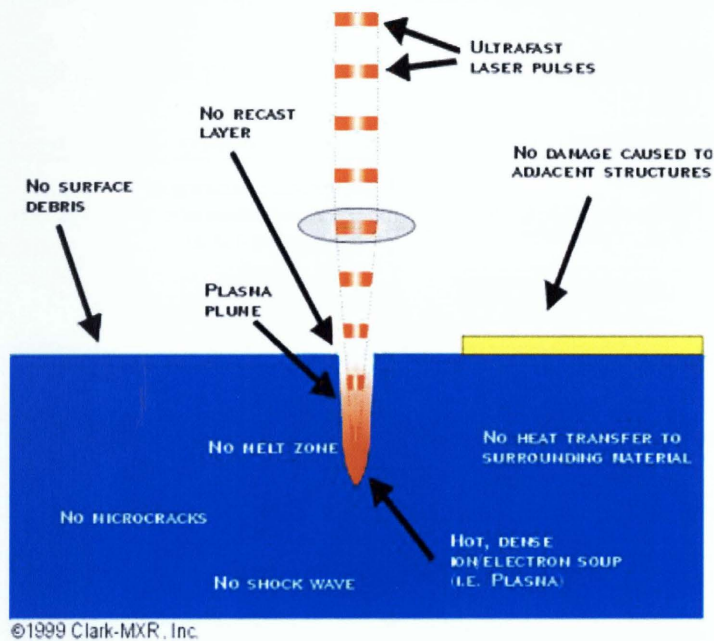


Figure 2-6: Ultrafast Pulse Laser-Matter Interaction [19]

There are obviously many advantages to using femtosecond lasers [20]. The shorter pulse width allows for decreased heat affected zone (HAZ) since there is less heat loss. The laser beam does not directly heat the substrate and the thermal effects are limited to the laser spot size. Also, it is possible to avoid interactions of the laser beam and the plasma formed during laser ablation. This leads to cleaner and finer cuts. Furthermore, with a well established set of parameters, the threshold fluence, Φ_{TH} , will remain constant leading to creation of features smaller than the spot size of the laser beam. These advantages of femtosecond laser pulses allow very precise and pure laser processing of silicon which is experimentally demonstrated in Chapters 4 and 5.

As [19] mentions, the major shortcoming of femtosecond lasers is low throughput due to low average power. However, newer models of femtosecond lasers have an average beam power > 20 W which means increased throughput and lowered cost of micro and nanomachining on a per-unit basis.

CHAPTER 3

EXPERIMENTAL SETUP

3.1 INTRODUCTION

Selection of laser system and understanding of the laser parameters are most essential for the laser nano-machining operation. In this chapter, an overview of the laser system selected for this study is provided. Also, the experimental setup used for this study is discussed. These experiments were conducted using a high repetition rate femtosecond laser system in the Micro and Nano Fabrication Research Lab at Ryerson University, Toronto, Canada.

3.2 EXPERIMENTAL SETUP

The experiments were carried out using a diode-pumped Yb-doped fiber oscillator/amplifier system capable of producing variable repetition rates of 200 kHz to 25 MHz with an average power output of 12 W at 2 MHz (Clark-MXR Inc. IMPULSE Series Ultrashort Pulse Laser). The Yb-doped fiber-oscillator/fiber-amplifier design allows for the low noise performance of solid state to be combined with high spatial mode quality of fiber lasers. The laser can produce pulses with duration between < 250 fs and 10 ps. The laser beam produced has a central wavelength of $1.03 \mu\text{m}$. All major laser parameters such as pulse width, repetition rate, total beam power are computer controlled. The laser beam diameter is expanded by a plano-convex lens of 500 mm focal length and a plano-concave lens of 150 mm focal length. A $\frac{\lambda}{2}$ wave-plate in between the two optical lenses is used to control the polarization of the beam before being converted to the second harmonic (515 nm) central wavelength using a harmonic generator. As others have demonstrated as well, the light frequency doubling from 1030 nm to

515 nm greatly increased the efficiency and ease with which the micromachining of the features were carried out due to the reduction in the order of multiphoton absorption [21]. The second harmonic is more capable of creating nanometric features. Afterwards, three 515 nm mirrors were used to dump the 1030 nm wavelength out of the beam. In addition, a plano-concave lens of 75 mm focal length and a plano-convex lens of 300 mm focal length are utilized to increase the beam diameter by 4 times to 8 mm. A $\frac{\lambda}{4}$ wave-plate in between the two optical lenses ensures circular polarity of the beam. A diaphragm is used to perfect the beam profile. Next, the beam is scanned onto the sample surface using a uniquely designed piezo tip/tilt mirror. The 16 mm diameter, 2 mm thick mirror consists of 2 fixed orthogonal axes with a common pivot point [22]. The common pivot eliminates the so-called pillow effect and hence field distortion at the image plane is avoided and compensation software to remove the distortion is not required. The novel lever design allows for an exceptional tip/tilt range of 50 mrad ($\sim 3^\circ$) with sub μ rad resolution which translates to a beam deflection of up to 100 mrad ($\sim 6^\circ$) [22]. This parallel-kinematics design allows for a smaller package with faster response and better linearity with equal dynamics for both axes [22]. The mirror also incorporates zero friction, zero stiction flexure guides and has a high resonant frequency of 1 kHz [22]. This is critical for high repetition rate laser machining since precise pulse number control demands for high frequency beam steering. The frictionless guides and drives do not experience wear and tear which in turn leads to an exceptionally high level of reliability [22]. Finally, the beam is focused onto the sample surface using a telecentric lens with a 12.478 mm focal length [23]. The theoretical laser machining spot diameter (D_0) was calculated from $D_0 \approx 1.27 \frac{\lambda_0 f}{D}$ [24]. Here, f is the effective focal length of the telecentric lens equal to 12.478 mm, λ_0 is the wavelength of the laser equal to

515 nm and D is the laser beam diameter equal to 8 mm. From this formula the theoretical spot size is calculated to be 1.02 μm in diameter.

The telecentric lens ensures that the laser hits the sample surface at 90° over the entire scanning field thus projecting the correct spot size and wall angle for the application in this study [23]. The gold-coated silicon wafers used in Chapter 4 as well as the normal silicon wafers used in Chapter 5 are mounted on a two-axis (x and y) translation stage with a precision of 0.5 μm . The silicon wafer samples used in this study were P type Boron doped silicon wafer of 50 mm diameter, back grinded to 250 μm thickness with orientation of $\langle 100 \rangle$. The gold-coated silicon wafer samples have a thin film thickness of 3000 \AA and a substrate thickness of 250 μm . Each line on the workpiece was cut with only one pass scan. The analysis of the samples for quality, structure and removed material was carried out under a scanning electron microscope (SEM). Figure 3-1 is the schematic drawing of the experimental setup. All experiments were carried out in ambient atmosphere inside a temperature/humidity controlled room.

1. 1030 nm Mirror
2. F = 500 mm Convex Lens
3. 1030 nm $\lambda/2$ Waveplate
4. F= -150 mm Concave Lens
5. 515 nm Harmonic Generator
6. 515 nm Mirror
7. 515 nm Mirror
8. F= -75 mm Concave Lens
9. 515 nm $\lambda/4$ Waveplate
10. F = 300 mm Convex Lens
11. 515 nm Mirror
12. Diaphragm
13. Piezo Scanner
14. EFL = 12.478 mm Telecentric Lens
15. Sample and Sample Holder

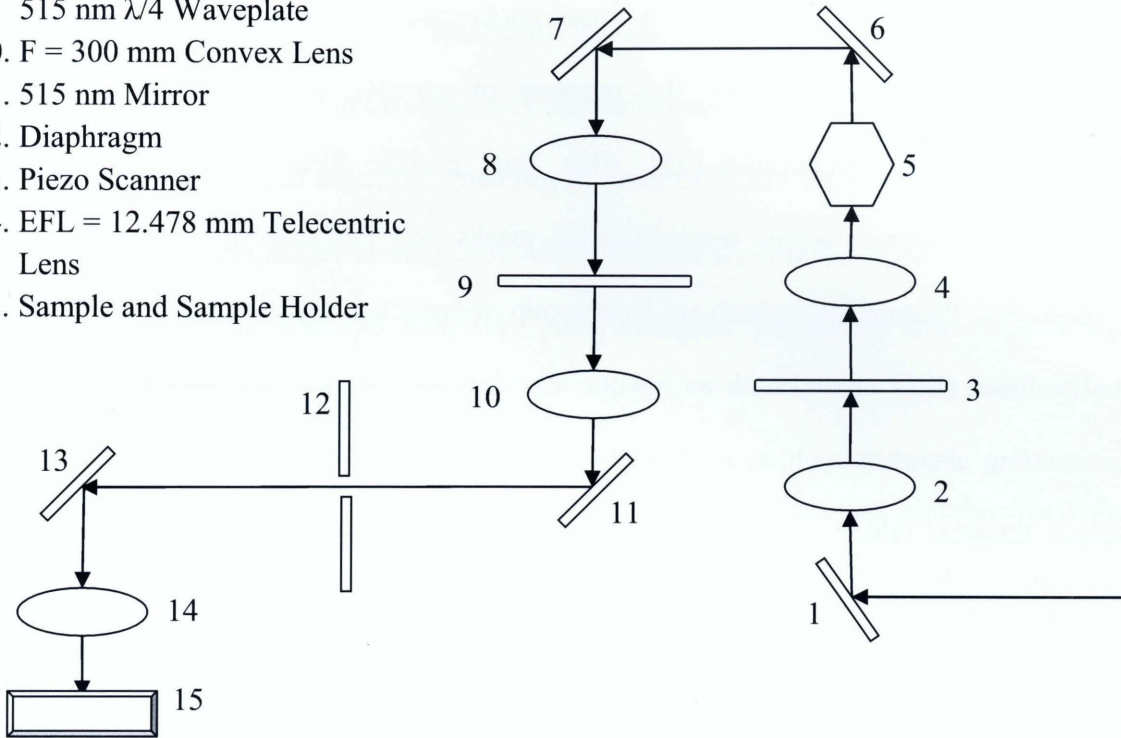


Figure 3-1: Experimental Setup

CHAPTER 4

EFFECT OF REPETITION RATE

4.1 INTRODUCTION

Thin film micro-machining has found application in different fields. Thin metallic films have been micro-machined for the purpose of creating high density data storage and semiconductor microelectronics [25]. Also, thin metallic films coated on glass are micro-machined in order to repair semiconductor masks and fabricate opto-electrical and MEMS devices [26]. Photomasks, which are a subgroup of semiconductor masks, are composed of high quality fused silica coated with an opaque absorber such as 100 nm thick Cr layer or partially transmitting absorber such as molybdenum silicide [27]. The defects usually take the form of excess absorber which when transferred to the wafer result in writing errors that cause the integrated circuit to malfunction [27]. Since the manufacturing process for photomasks is very expensive, up to \$100K for complex masks, defect removal is highly desirable. Laser ablation is preferred over ion or electron beam due to the higher speed and also ability to work in atmospheric conditions [28]. Last but not least, in the solar energy industry, there are two concepts to build solar cells. One is rooted in traditional silicon micro-technology and the other in thin film technology where vapour deposition techniques are used to create integrated circuits on insulating substrates [29]. CuInSe₂ (CIS) is widely used as the absorber material for thin film solar cells [29, 30]. Laser ablation of thin films has demonstrated the ability to create finely defined micro-structures for solar cells [29].

There have been many studies conducted on the femtosecond laser ablation of thin films. As [19], [31] and [32] mention, there are several advantages to using femtosecond laser to conduct precision micro-machining. First of all, as the name suggests, the pulse width of these lasers is in the 10^{-15} seconds range. This characteristic leads to minimal heat diffusion into the work piece and creation of a small heat affected zone (HAZ). Therefore, the amount of debris and molten material left behind is insignificant leading to high quality machining finish. Furthermore, the laser threshold can be accurately controlled such that only a small section of the laser intensity is above ablation threshold enabling the user to create laser machining spot sizes smaller than the actual wavelength of the beam. Moreover, the short pulse width allows for very high peak intensities to be achieved with low pulse energies. Therefore, femtosecond laser machining is highly efficient.

Chirped Pulse Amplified (CPA) femtosecond laser systems are not suitable for nanomachining due to several significant shortcomings. These lasers are limited to kHz-level repetition rate, have high laser output power, are very complex and occupy large floor space. The system complexity leads to limited long-term stability and operation. In contrast, fiber laser systems do not suffer from such issues. The high repetition rate offered by these lasers along with the possibility to operate at low output powers make fiber lasers ideal for nanomachining.

The primary aim of this research will be to investigate the feasibility of using high repetition rate femtosecond laser for nanoscale material processing. The effect of pulse repetition rate and pulse energy on femtosecond laser machining of gold-coated silicon wafer was studied to determine the optimum values of each of these parameters for processing thin films. In this study, machined lines were analyzed and compared while varying the laser repetition rate from 1

MHz to 13 MHz. At each repetition rate, the average beam power was changed from a value well above the damage threshold down to the point where no machining occurred, namely, below the ablation threshold. The machined structures were analyzed under scanning electron microscope (SEM).

4.2 HEAT CONDUCTION AT HIGH PULSE REPETITION RATE

As [6] indicates, if one considers a single laser beam pulse heating a plane solid target in the heat conduction regime, then the losses due to radiation and plume expansion can be neglected. It can further be assumed that the laser energy will be absorbed in a layer much thinner than the penetration depth of the heat wave. Therefore, the one-dimensional heat conduction equation can be utilized to model the progression of the heat wave into the target [6]:

$$\frac{\partial T}{\partial t} = a \frac{\partial^2 T}{\partial x^2} \tag{Eq. 4-1}$$

Where:

$$a = \frac{k}{c_p \rho_0}$$

Here a is the thermal diffusion coefficient in $[\text{cm}^2/\text{s}]$, k is the heat conduction coefficient in $[\text{J}/(\text{s cm K})]$, C_p is specific heat $[\text{J}/(\text{g K})]$ and ρ_0 is target material density in $[\text{g}/\text{cm}^3]$.

As [6] mentions, if the laser profile is taken to be rectangular in shape with a step-like rise and fall and also assume that the target fills the half space at $x \geq 0$ as well as presume the heat flux at the target surface having the same temporal form as the absorbed laser flux, then the heat conduction equation, equation (4-1), with these boundary conditions, has an exact solution [6]:

$$T(x, t) = \frac{a^{1/2}}{k\pi^{1/2}} \int_0^{t_p} \frac{I_a(\tau)}{(t-\tau)^{1/2}} \exp\left\{-\frac{x^2}{2a(t-\tau)}\right\} d\tau \quad \text{Eq. 4-2}$$

If the temperature of the heated area of the target averaged over space to the end of the laser pulse as a function of the laser (for the rectangular shaped pulse) and target parameters is considered, then the time dependence of surface temperature during the laser pulse ($t < t_p$) can be written as [6]:

$$T(t) = T_m \left(\frac{t}{t_p}\right)^{1/2} \quad \text{Eq. 4-3}$$

Here, t_p is the laser pulse duration and T_m is the maximum surface temperature.

It should be noted that the maximum target temperature, T_{\max} or T_m , occurs at the end of the laser pulse, i.e. $T_{\max} = T(0, t_p)$.

To characterize the cooling of the target after the end of the laser pulse, the exact solutions of the heat conduction equation must be utilized to find the time dependence of the surface temperature after the end of the laser pulse [6]:

$$T(0, t) = T(0, t_p) \left(\frac{t_p}{t}\right)^{1/2} = \sqrt{\frac{2}{\pi}} \frac{I_a (at_p)^{1/2}}{k} \left(\frac{t_p}{t}\right)^{1/2} \quad \text{Eq. 4-4}$$

Where, I_a is the absorbed laser intensity, t_p is the laser pulse duration, a is the thermal diffusion coefficient, k is the heat conduction coefficient

For the application considered in this thesis, it is imperative to consider the target surface temperature for the case of a succession of laser pulses rather than only one pulse. According to [6], the target surface temperature after n laser pulses of pulse duration t_p following with time

intervals t_{pp} can be calculated as follows. The maximum temperature at the end of a single laser pulse is T_{max} and the temperature at the beginning of the following laser pulse is $T_{min} = T_{max}(t_p/t_{pp})^{1/2}$. For all laser pulses with the fixed repetition rate, the ratio for the previous maximum and the following minimum is constant and equal to $\alpha = (t_p/t_{pp})^{1/2}$. From the above relationships, the maximum and minimum temperature of the target surface for a succession of n laser pulses can be easily calculated [6]:

$$\begin{aligned}
 \text{First Pulse:} \quad & (T_{max})_1 = T_m \quad ; \quad (T_{min})_1 = \alpha T_m; \\
 \text{Second Pulse:} \quad & (T_{max})_2 = (1 + \alpha)T_m \quad ; \quad (T_{min})_2 = \alpha(1 + \alpha)T_m; \quad \text{Eq. 4-5} \\
 \text{nth pulse:} \quad & (T_{max})_n = (1 + \alpha + \alpha^2 + \alpha^3 + \dots + \alpha^{n-1})T_m \\
 & = [(1 - \alpha^n)/(1 - \alpha)]T_m \approx (1 - \alpha)^{-1}T_m; \\
 & \text{and } (T_{min})_n = \alpha(T_{max})_n.
 \end{aligned}$$

These equations can be derived in such a manner due to the linear nature of the heating process.

After several derivations, [6] concludes that the average surface temperature after n pulses is:

$$\bar{T}_n = \frac{1}{n(t_p+t_{pp})} \int_0^{n(t_p+t_{pp})} T(0,t)dt = 2\alpha \frac{(1-\frac{2}{3}\alpha)}{(1+\alpha^2)} \cdot \frac{1}{n} \sum_{i=1}^n \bar{T}_{max,i} \quad \text{Eq. 4-6}$$

Where
$$\sum_{i=1}^n \bar{T}_{max,i} = T_m \left(1 + \frac{1-\alpha^2}{1-\alpha} + \dots + \frac{1-\alpha^n}{1-\alpha} \right) = \frac{T_m}{(1-\alpha)} \left(n + \frac{\alpha^n - \alpha}{1-\alpha} \right)$$

The average temperature takes the final form [6]:

$$\bar{T}_n = 2\alpha \frac{\left(1 - \frac{2}{3}\alpha\right)}{(1+\alpha^2)} \cdot \frac{T_m}{(1-\alpha)} \left(1 + \frac{\alpha^n - \alpha}{n(1-\alpha)}\right) \quad \text{Eq. 4-7}$$

In the case of $n \gg 1$ and $\alpha \ll 1$ [6]:

$$\bar{T}_n \cong 2\alpha T_m = 2T_m \left(\frac{t_p}{t_{pp}}\right)^{1/2} \quad \text{Eq. 4-8}$$

Therefore, the average target surface temperature is proportional to the maximum surface temperature T_m reached at the end of the laser pulse in a single-pulse regime and the square root of the product of the pulse duration t_p and the laser repetition rate t_{pp} [6].

If the average thin film surface temperature for 214 fs and a high laser repetition rate of 116 MHz using equation (4-8) is calculated, the following result is obtained:

$$t_p = 214 \text{ fs}; R_{\text{rep}} = 116 \text{ MHz or } t_{pp} = 0.0086 \mu\text{s}$$

$$\bar{T}_n \cong 2\alpha T_m = 2T_m \left(\frac{t_p}{t_{pp}}\right)^{1/2} = 2T_m \left(\frac{214 * 10^{-15}}{0.0086 * 10^{-6}}\right)^{1/2} = 0.01T_m$$

Where:

$$\alpha = \left(\frac{t_p}{t_{pp}}\right)^{1/2} = \left(\frac{214 * 10^{-15}}{0.0086 * 10^{-6}}\right)^{1/2} = 0.005$$

As this calculation indicates, even at the high laser repetition rate of 116 MHz, the gold thin film cools off between the pulses and only retains 1% of the maximum surface temperature T_m . Thus, it is expected that the heat accumulation will be minimal in the experiments conducted in this study which range from 1 MHz to 13 MHz with the same 214 fs pulse width.

Furthermore, this calculation shows that truly for femtosecond lasers, there is minimal heat diffusion into the work piece and a small heat affected zone.

4.3 RESULTS AND DISCUSSION

4.3.1 EFFECTS OF LASER FLUENCE CHANGE ON CRATER WIDTH AND HEAT AFFECTED ZONE

Figure 4-1 craters were created at 13 MHz at various energy levels. For instance, for fluence of 3.340 J/cm^2 , 2.672 J/cm^2 and 2.042 J/cm^2 , the crater width is approximately 340 nm, 150 nm and 110 nm respectively. As evident from the SEM pictures, the lower the energy fluence is, the smaller the crater width will be. The same is true for the heat affected zone which changes from $1.20 \text{ }\mu\text{m}$ to $1.18 \text{ }\mu\text{m}$ and $0.79 \text{ }\mu\text{m}$. The heat affected zone is defined as the area surrounding the crater which has had its microstructure and properties changed during the laser ablation process. In the SEM images, it is identified as the raised area with a distinct morphology profile running along both sides of the crater. The crater width and the HAZ were measured in 5 different points and the result was averaged to give the final crater width and HAZ measurement for a particular SEM image. The crater width varies by as much as 46% at 3.340 J/cm^2 compared to 18% at 2.042 J/cm^2 . This can be attributed to the fact that at lower fluence, the pulse energy is lower as well. Therefore, the variation in one pulse with respect to another has a lesser impact on the crater width.

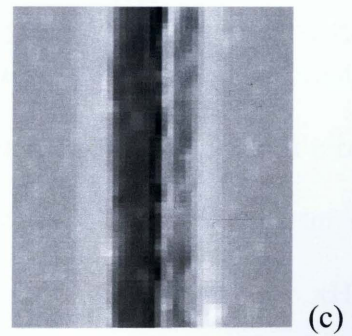
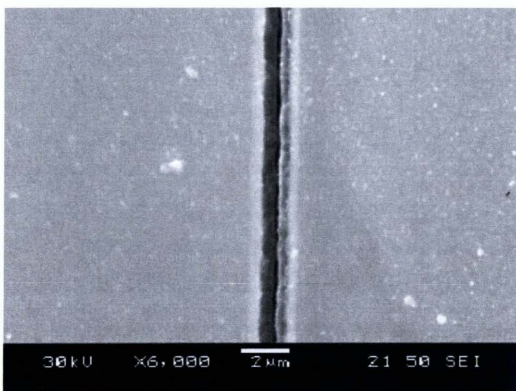
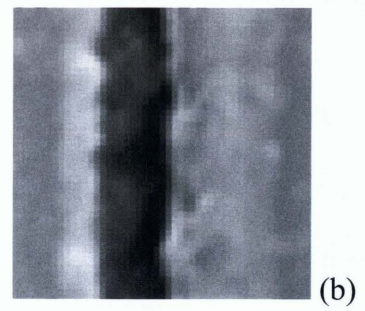
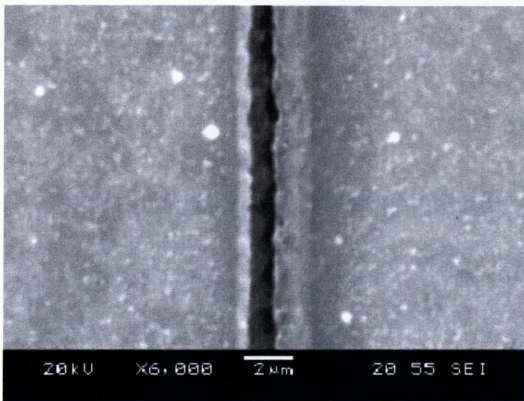
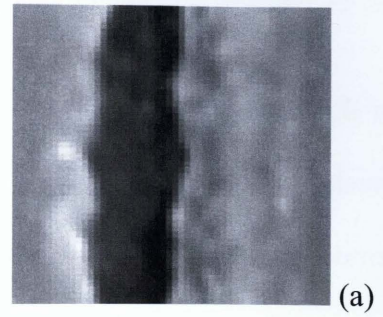
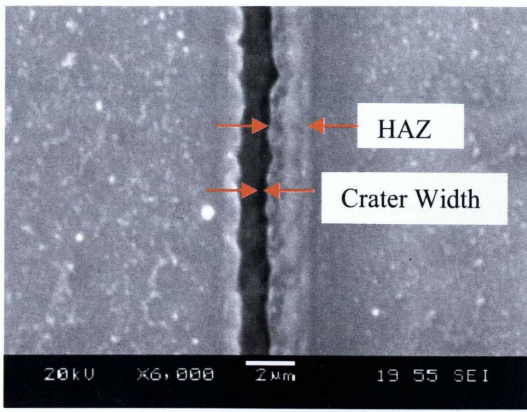


Figure 4-1: All images at 13 MHz laser repetition rate. (a) SEM image of 3.340 J/cm² fluence (b) SEM image of 2.672 J/cm² fluence (c) SEM image of 2.042 J/cm² fluence

4.3.2 EFFECTS OF PULSE REPETITION RATE ON ABLATION THRESHOLD

Graphs demonstrating the threshold energy fluence and threshold average beam power for different laser repetition rates were plotted (Figures 4-2 and 4-3). As seen in Figure 4-2, the threshold fluence decreases rapidly with increase in the laser repetition rate. However, at a certain point, the threshold fluence reaches saturation and no longer decreases with an increase in the repetition rate. This result agrees well with those obtained by other authors [33]. However, the higher the laser repetition rate is, the higher the threshold average beam power becomes as shown in Figure 4-3.

As the laser repetition rate increases, the effective number of pulses incident on the center of the cut, N_{eff} , increases while the pulse energy decreases. The effective number of pulses incident at the center of the cut, N_{eff} , was calculated from [34]:

$$N_{eff} = \sqrt{\frac{\pi \omega_0 f}{2 v}} \quad \text{Eq. 4-9}$$

Where, ω_0 is the machining spot radius which is equal to 0.51 μm , f is the laser repetition rate and v is the feed rate (piezo scanning speed) which is constant at 4000 $\mu\text{m/s}$. N_{eff} was calculated for instance to be 2078 pulses for 13 MHz, 1386 pulses for 8.67 MHz and 1039 pulses for 6.50 MHz.

The increase in N_{eff} leads to a decrease in the laser energy fluence required to initiate ablation (Figure 4-2). It is important to note that Figure 4-2 flats out after repetition rate of 5 MHz and remains at a constant threshold fluence. This is due to the fact that a minimum threshold fluence is required to start the ablation process. If the laser fluence goes below this

minimum threshold fluence, no ablation occurs no matter how many pulses are fed to the target surface [22]. Therefore, as Figure 4-3 demonstrates, while the threshold fluence remains almost constant, increase in the pulse repetition rate leads to the increase in threshold laser power.

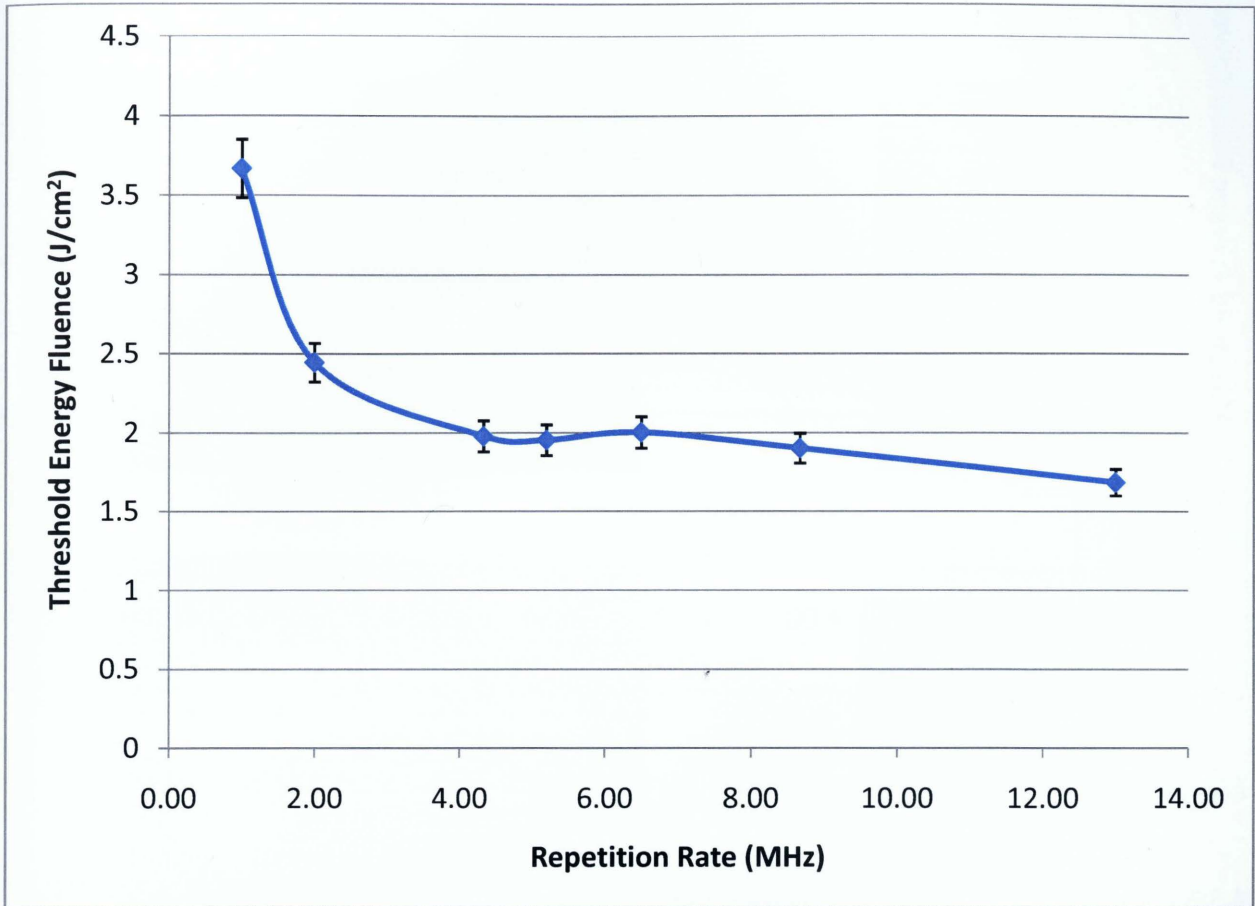


Figure 4-2: Threshold Energy Fluence vs. Repetition Rate from 1 MHz to 13 MHz

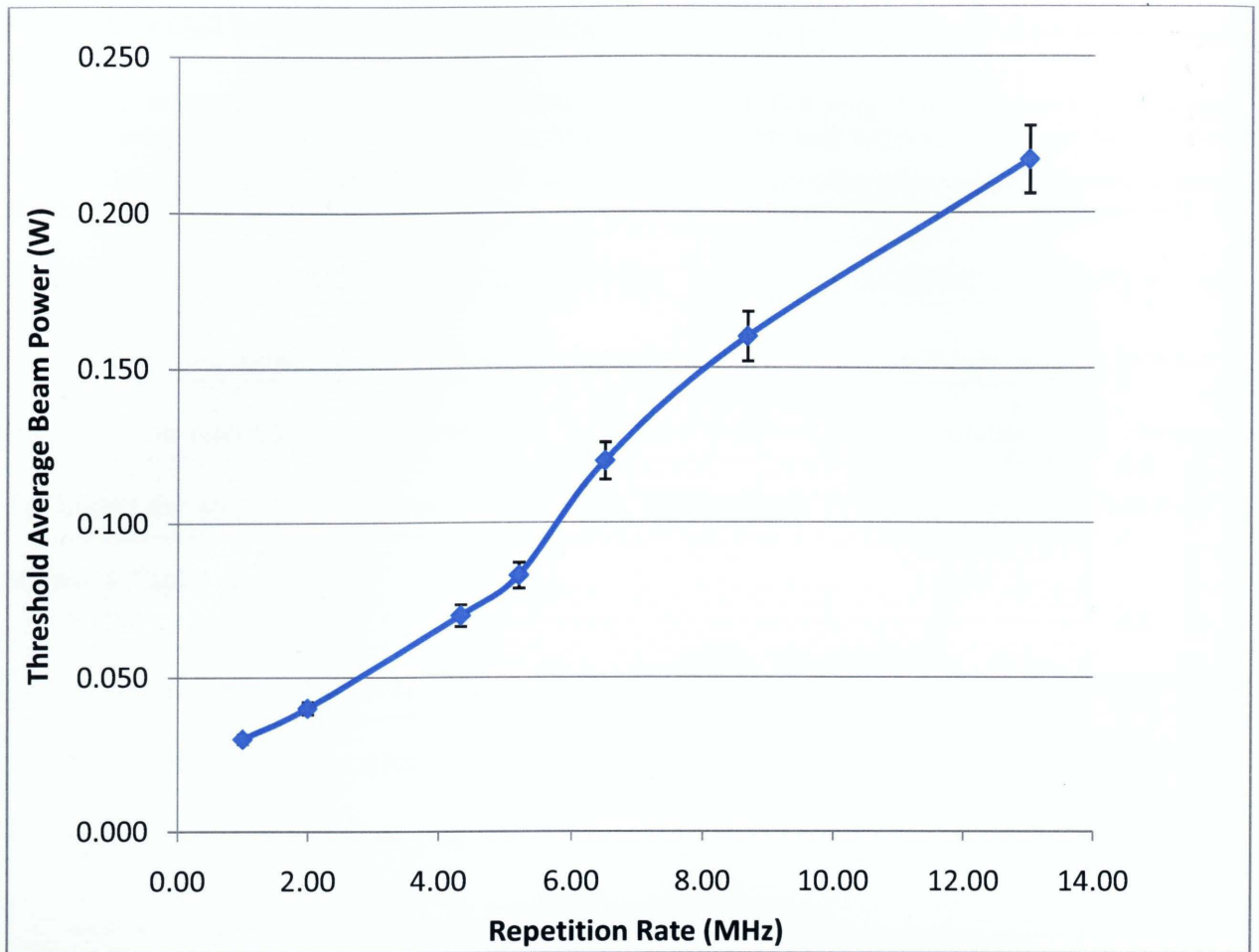


Figure 4-3: Threshold Average Beam Power vs. Repetition Rate from 1 MHz to 13 MHz

4.3.3 EFFECTS OF PULSE REPETITION RATE ON CRATER WIDTH AND HEAT AFFECTED ZONE

As shown in Figure 4-4, at a constant fluence of 2.917 J/cm^2 , the crater width decreases as the laser repetition rate increases. For instance at 4.33 MHz and 5.20 MHz, the crater width is 180 nm and 160 nm, respectively. It is important to note that although the effective number of pulses incident on the center of the cut, N_{eff} , is higher for 5.20 MHz, the feature size is smaller. The heat affected zone is smaller at 5.20 MHz as well. The crater width varies by as much as 40% at 4.33 MHz compared to 33% at 5.20 MHz. Also, at 5.20 MHz, the crater has a smoother

edge and the line width is more uniform. N_{eff} is higher at higher laser repetition rates which means there are more pulses impacting the sample surface. Therefore, better overlapping occurs which leads to a smoother cutting edge. The high N_{eff} also means that the variation in one pulse with respect to another has a lesser impact on the crater width.

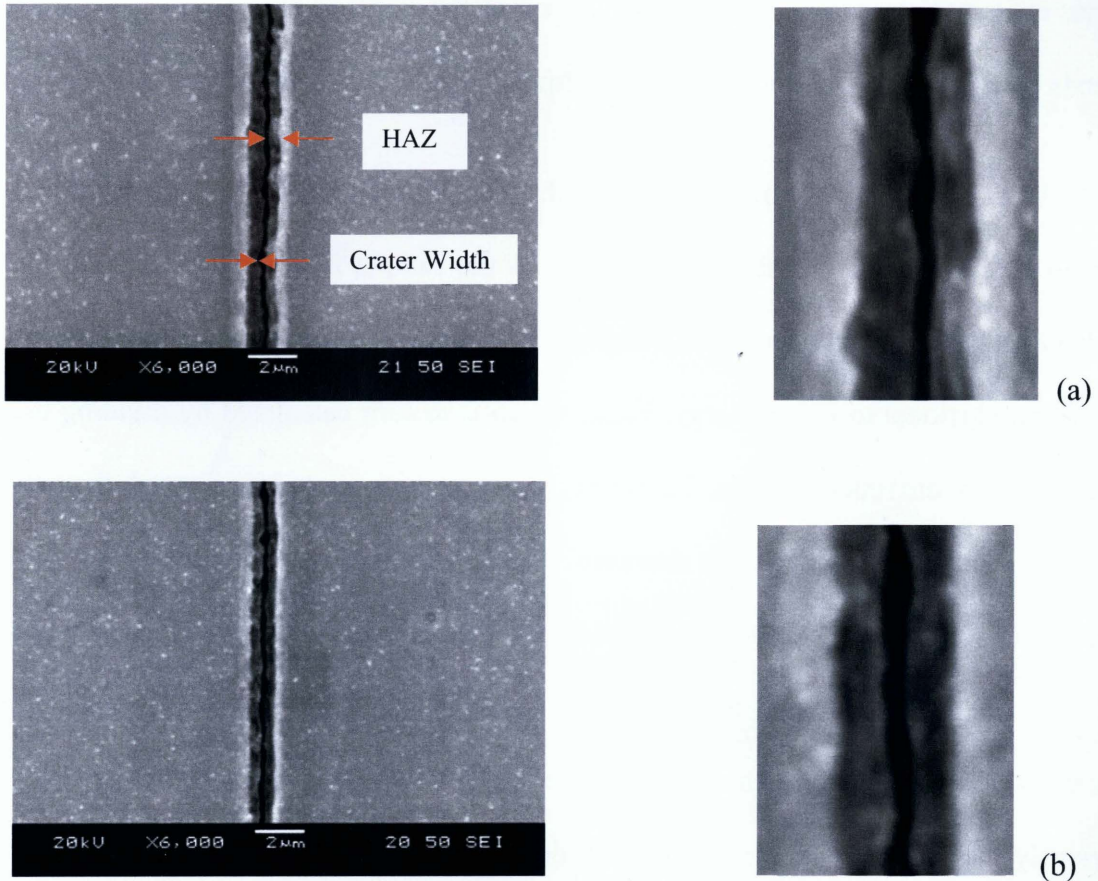


Figure 4-4: All images at fluence of 2.917 J/cm^2 . (a) SEM image of 4.33 MHz repetition rate
 (b) SEM image of 5.20 MHz repetition rate

The maximum laser fluence (peak fluence), φ_0 , is related to the measured pulse energy

E_{pulse} by [33]:

$$\varphi_0 = \frac{2E_{\text{pulse}}}{\pi\omega_0^2} \tag{Eq. 4-10}$$

For lasers with a Gaussian beam profile, the feature size is related to the maximum laser fluence, φ_0 , on the sample surface by [33]:

$$D^2 = 2\omega_0^2 \ln\left(\frac{\varphi_0}{\varphi_{th}}\right) \quad \text{Eq. 4-11}$$

Where, ω_0 is the machining spot radius and φ_{th} is the material modification threshold, which depends both on the material as well as the number of pulses incident on each machining point.

As indicated by previous researchers, the peak fluence of the laser spot must be precisely controlled at 2% above the ablation threshold of the sample in order to achieve a feature size one-tenth of the machining spot [32]. Equation 4-10 demonstrates that the peak fluence, φ_0 , is directly proportional to pulse energy, E_{pulse} , which is in turn calculated by dividing the average beam power by the repetition rate. Therefore, as the repetition rate is increased, the pulse energy and the peak fluence of the laser decrease. This means that only the center (or peak) of the Gaussian laser beam is above the material ablation threshold. As the repetition rate is increased further, a yet smaller central portion of the beam has fluence above the ablation threshold. Therefore, increasing the laser repetition rate should lead to a decrease in the crater width. Obviously, as the average beam power is decreased for a constant repetition rate, the pulse energy decreases, this again leads to a decrease in the peak fluence of the laser and a smaller crater width.

Crater width with respect to energy fluence at different repetition rates was plotted in Figure 4-5. As can be seen from Figure 4-5, a higher repetition rate is more capable of producing smaller craters. Also, the lower the energy fluence for a given repetition rate, the smaller the crater width. As shown in Figure 4-2, threshold fluency remains almost constant at repetition rate

higher than 5 MHz. Therefore, the portion above the ablation threshold reduces with increase in the repetition rate, which in turn results in a smaller feature size.

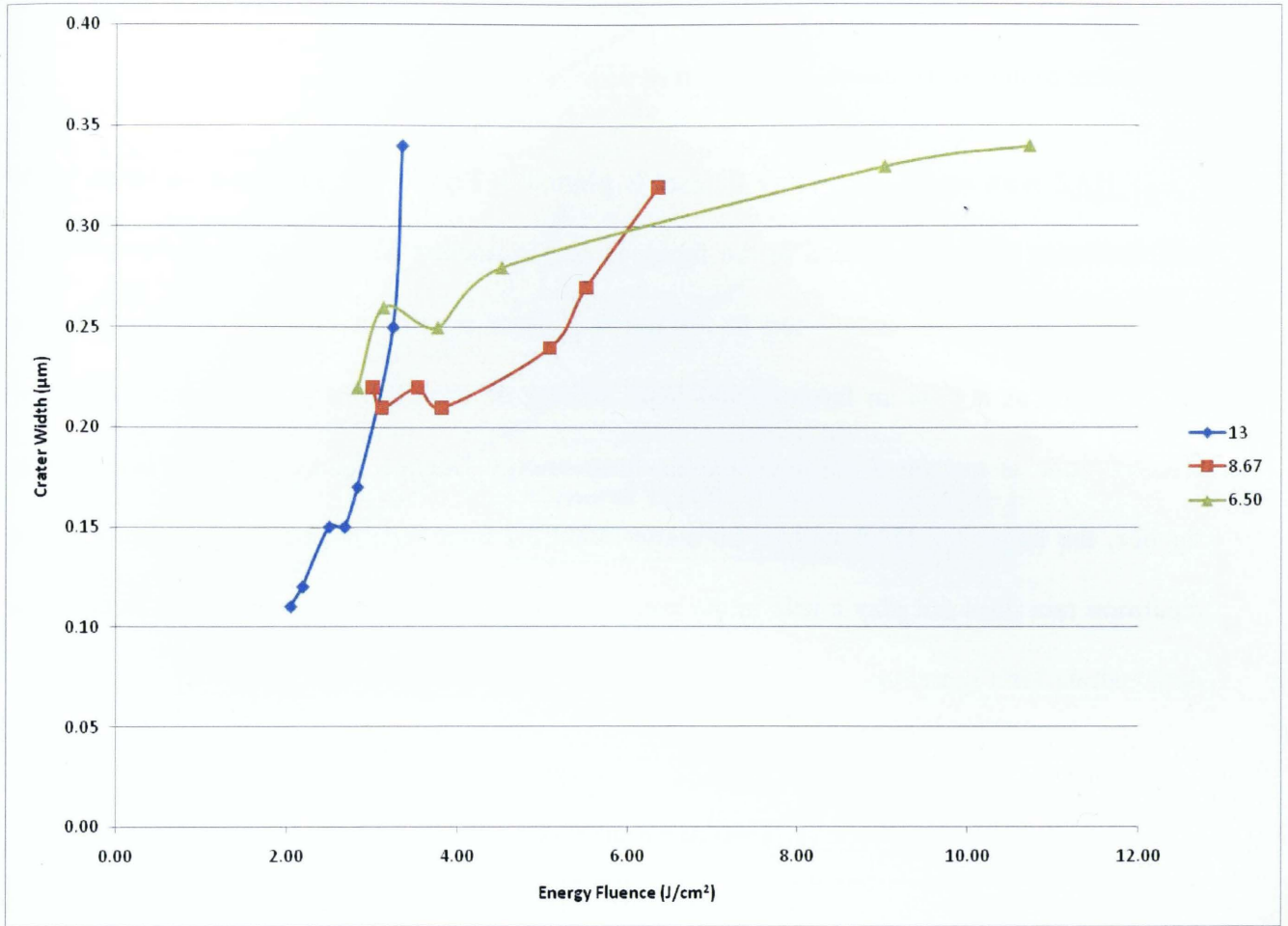


Figure 4-5: Crater Width vs. Energy Fluence for 6.50 MHz to 13 MHz laser repetition rate

The same phenomenon can be explained through the number of effective pulses incident at the center of the cut, N_{eff} . In this study's experiments, the feed rate, v , is constant at 4000 $\mu\text{m/s}$. Therefore, as the repetition rate increases, the N_{eff} increases as well. This leads to a decrease in the ablation threshold of the material, ϕ_{th} , as reported by other authors [33]. At the same time, the increase in repetition rate leads to a drastic decrease in the pulse energy, E_{pulse} ,

and the peak fluence, φ_0 , of the laser. As other researchers have mentioned, [35, 36], the change in the repetition rate and therefore peak fluence greatly outweighs the change in the number of incident pulses, N_{eff} . Therefore, overall, the $\frac{\varphi_0}{\varphi_{th}}$ ratio decreases. This leads to a decrease in the feature size diameter, D , based on equation (4-11).

HAZ with respect to energy fluence is plotted in Figure 4-6. The great variation in the measurements of the HAZ seen in the figure is due to unclear SEM images and fluctuation in laser beam profile. As mentioned in section 4.2, laser repetition rate will not lead to heat accumulation as it does in femtosecond laser writing of waveguides [35]. Therefore, the heat affected zone is mainly determined by the laser energy fluence. The higher the laser energy fluence, the larger the HAZ will be no matter what the laser repetition rate is. Therefore, laser repetition rate does not play a role in the size of the HAZ for different laser energy fluencies as demonstrated in Figure 4-6.

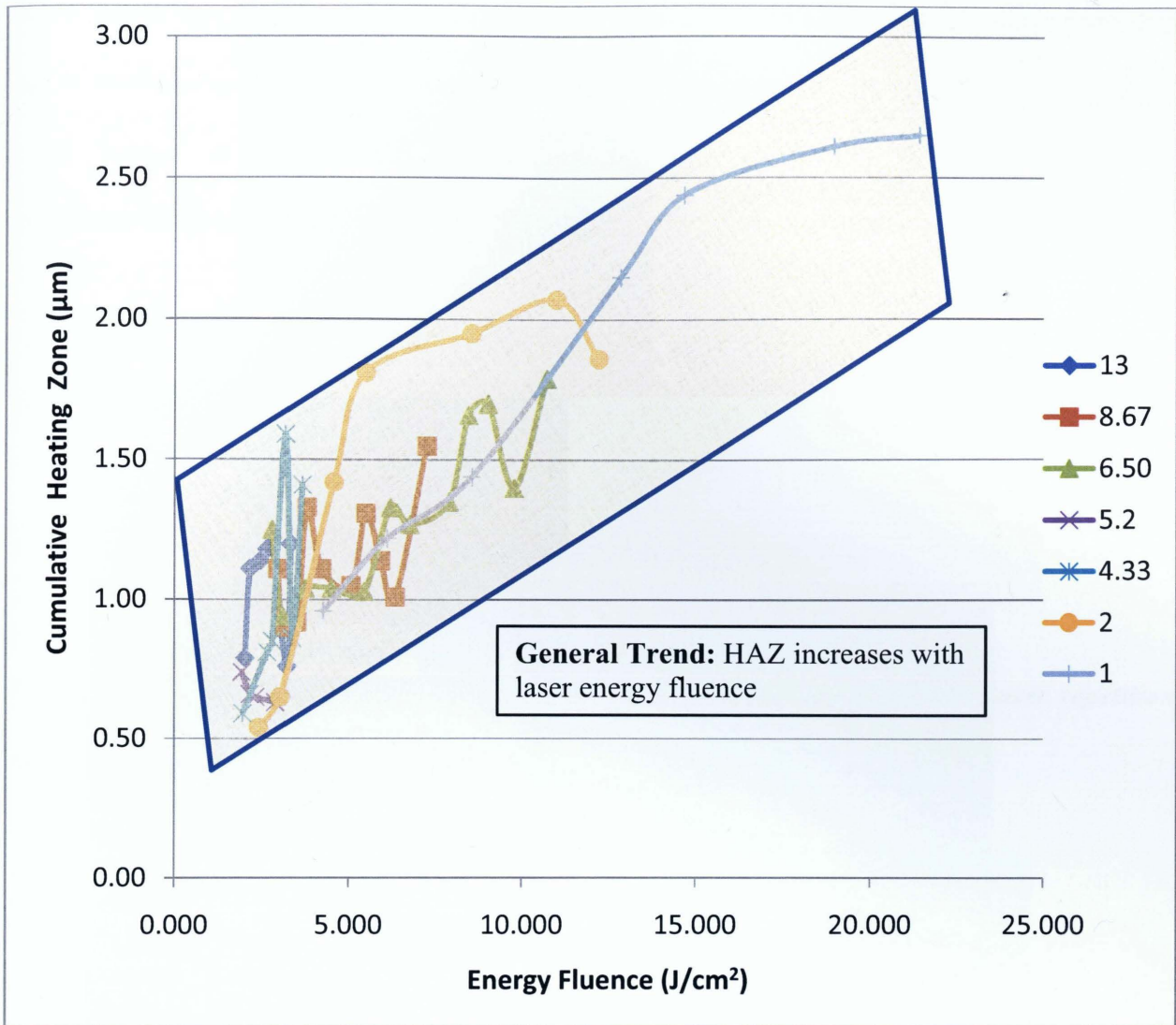


Figure 4-6: Heat Affected Zone vs. Energy Fluence for 1 MHz to 13 MHz laser repetition rate

Figures 4-7, 4-8 and 4-9 pertain to the smallest features obtained for 6.50 MHz, 8.67 MHz and 13 MHz respectively. For Figure 4-7, the crater width is measured to be 220 nm and the heat affected zone is 1.25 µm. The experiment was carried out at 2.822 J/cm² beam energy fluence and 6.50 MHz laser repetition rate. In Figure 4-8, the crater width is measured to be 180 nm and the cumulative heating zone is 1.11 µm. The experiment was carried out at 2.991 J/cm² beam energy fluence and 8.67 MHz laser repetition rate. Finally, in figure 4-9, the crater width is

measured to be 110 nm and the heat affected zone is 0.79 μm . The experiment was carried out at 2.042 J/cm^2 beam energy fluence and 13 MHz laser repetition rate. The pattern waviness is due to the laser system not being enclosed completely. However, it is located in a temperature/humidity controlled room. The crater width change is due to power fluctuation of the laser.

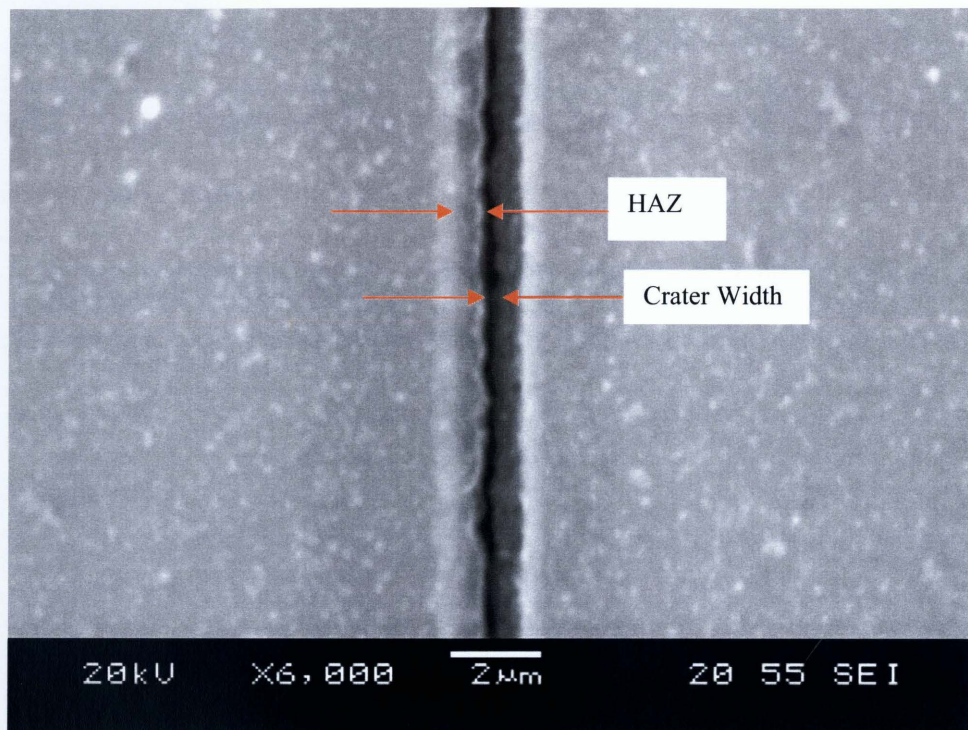


Figure 4-7: SEM image of 2.822 J/cm^2 beam energy fluence and 6.50 MHz laser repetition rate cutline with crater width of 220 nm and heat affected zone of 1.25 μm

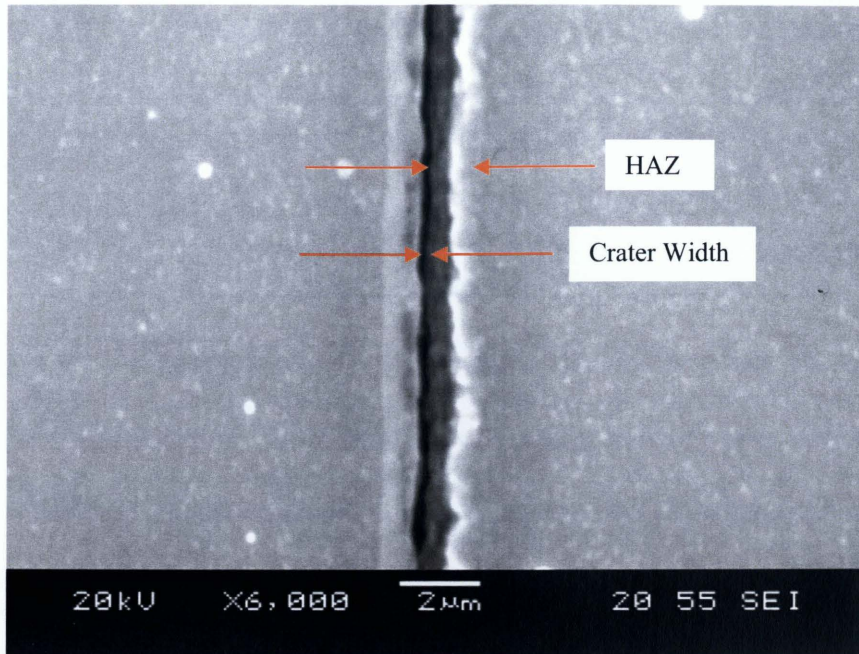


Figure 4-8: SEM image of 2.991 J/cm² beam energy fluence and 8.67 MHz laser repetition rate cutline with crater width of 180 nm and heat affected zone of 1.11 µm

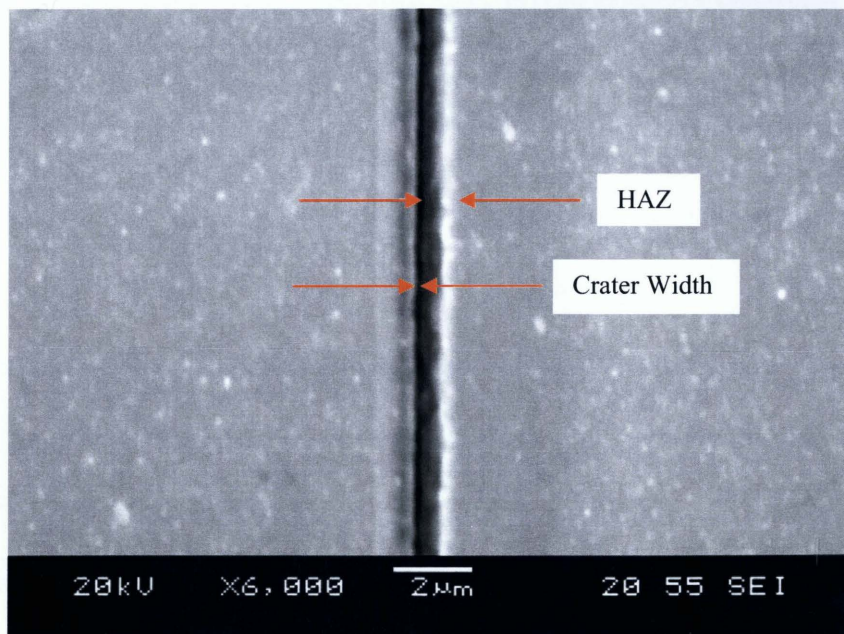


Figure 4-9: SEM image of 2.042 J/cm² beam energy fluence and 13 MHz laser repetition rate cutline with crater width of 110 nm and heat affected zone of 0.79 µm

4.4 SUMMARY

Thin film laser micromachining has been utilized for repairing semiconductor masks, creating solar cells and fabricating MEMS devices. A unique high repetition rate femtosecond fiber laser system capable of variable repetition rates from 200 kHz to 25 MHz along with helium gas assist was used to study the effect of pulse repetition rate and pulse energy on femtosecond laser machining of gold-coated silicon wafer. It was seen that high repetition rates lead to smaller craters with uniform line width. Craters created at 13 MHz pulse repetition rate with 2.042 J/cm^2 beam energy fluence measured 110 nm in width and had a heat affected zone of $0.79 \text{ }\mu\text{m}$. It was found that pulse repetition rate did not play a significant role in the size of the heat affected zone. The HAZ became larger with increase in the laser energy fluence no matter what the laser repetition rate was. In the future, a 1 W laser system will be acquired to find the optimal repetition rate that would create the minimal feature size with the least heat affected zone. Using this kind of setup, along with techniques such as radial polarization and a different gas assist, may enable the creation of sub 100 nm feature size with good quality.

CHAPTER 5

SILICON WAFER SURFACE PATTERNING USING FEMTOSECOND LASER IRRADIATION BELOW ABLATION THRESHOLD

5.1 INTRODUCTION

Surface patterning using femtosecond laser has many applications such as fabrication of MEMS/NEMS, CMOS, 3D-microstructures, micro trenches, micro channels, micro holes, periodical submicron gratings and nanophotonics [37, 38]. Also, the laser maskless patterning of magnetic thin films and transparent electrode films can be used for microelectronics applications such as fabrication of flat panel displays and hard disk drives [39]. As electronic components become more compact, the miniaturization of these devices requires a large scale and fast patterning technique.

According to [38, 39], there are various micro-patterning techniques such as electron beam etching, photolithography, atomic force microscopy, soft lithography, laser micromachining and microsphere nanopatterning. Electron beam etching produces too much heat and damage while photolithography involves multiple steps and requires the use of chemicals. Atomic force microscopy takes advantage of mechanical forces to etch the surface, but the procedure is slow and cannot conveniently etch large surface areas. Soft lithography techniques such as microcontact printing, micromolding, microtransfer moulding and replica moulding, imprinting and injection molding can be used due to their low thermal effect, cost and the ability to scan a large area. However, these techniques do involve multiple steps and require specialized

masters. Laser micromachining is preferred because of fast material processing speed, large scan area and single-step capability. Microsphere nanopatterning in which laser light is focused through a layer of self-assembly microparticles is capable of creating submicron periodic patterns. The major disadvantages include difficulty in controlling the particle arrangement and the particles cannot be used repeatedly.

As [40] points out, the femtosecond pulse laser is advantageous for pattern formation. The shorter pulse width generates smaller bubbles which have a shorter period of oscillation and cause a ripple pattern before the melted silicon surface solidifies. Also, the shorter pulse width lowers the energy conversion efficiency from light energy to a shockwave. The shockwave moves a bubble or causes it to collapse but the effect is negligible for pulse width shorter than 300 femtosecond.

As [7] demonstrated, amorphization, melting, re-crystallization, nucleated vaporization and ablation occur as part of the laser machining of silicon wafers. Features such as bubbles as well as ripples and columns are created during these stages. The resolidification happens in two stages: amorphization and recrystallization. The main difference between these two processes rests with amount of energy deposited in the material in temperature form and the following cooling velocity. At lower temperatures, characterized by short irradiation periods, the material does not re-crystallize after melting and remains in an amorphous state. However, if the temperature is high enough, then the slow cooling will permit re-crystallization.

Figure 5-1, [7], illustrates the diverse surface features that can occur at different thresholds of the silicon wafer. It further demonstrates the dependence of these concepts on the laser fluence and number of laser pulses illuminating the silicon surface. The threshold fluences for each of these phenomena can be calculated by measuring the diameter of the modified areas

versus the pulse fluence and extrapolating to zero. As the figure demonstrates, as the laser fluence increases beyond the ablation threshold, at a moderately high laser pulse number, the ripples give way to columns. If the number of laser pulses is very low, then bubbles form when the laser fluence passes the ablation threshold. The modification threshold refers to the laser fluence required to initiate the amorphization process, namely, changing the silicon surface from solid to liquid. After melting, re-crystallization of the liquid silicon layer occurs [41]. Of course, if the laser fluence is above the ablation threshold, the silicon wafer is machined. In our experiments, the ripples formed at a laser fluence range of 1.56 J/cm² to 4.66 J/cm² while grains formed at a laser fluence range of 3.34 J/cm² to 6.77 J/cm².

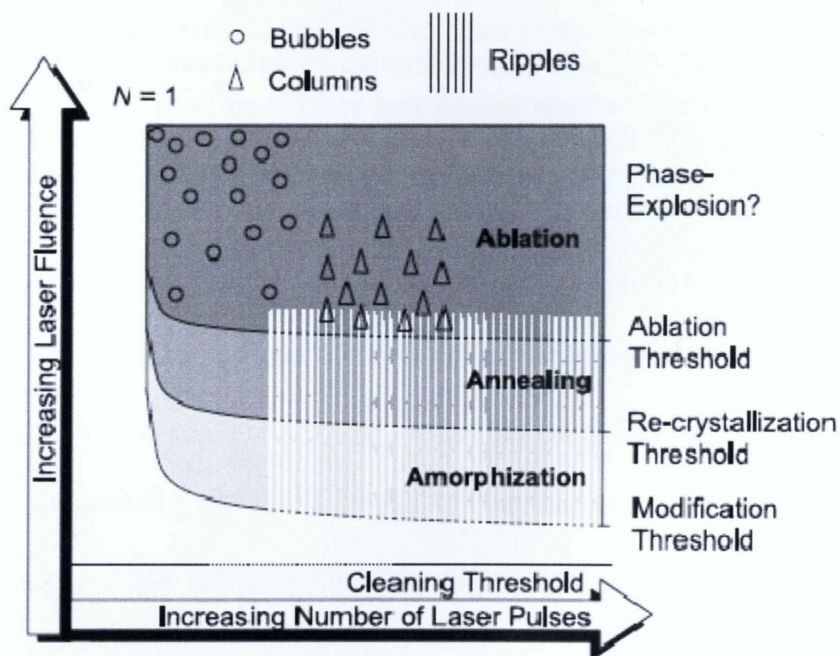


Figure 5-1: Scheme of the different morphological phenomena after irradiation of silicon surface with linearly polarized femtosecond laser pulses of typically 100 fs duration [7]

5.2 RESULTS AND DISCUSSION

5.2.1 RIPPLES

5.2.1.1 RIPPLE FORMATION MECHANISMS

In the ensuing sections, several mechanisms for formation of ripples have been described. The acoustic wave, surface tension gradient, interference between the incident light/surface wave and the Boson Condensation Hypothesis mechanisms have been described in detail. Except for the Boson Condensation Hypothesis which pertains to the femtosecond regime, the other mechanisms are associated with the picosecond laser pulse width.

5.2.1.1.1. ACOUSTIC WAVE

According to [42, 43], silicon goes through volume contraction and generates an acoustic wave upon melting. The thermoelasticity of silicon creates the acoustic wave even before melting with a power spectrum that peaks around the inverse of the pulse duration. Above the threshold, the generated sound wave lasts over several periods and consequently washes out. The acoustic wave propagates on the surface in an anisotropic manner. In [42], the ripples appeared parallel to one of the [110] crystal axes. However, in [43], the ripples are seen to be perpendicular to the laser polarization. The ripples are in fact a frozen out surface acoustic wave with a frequency of inverse the pulse width of the illuminating laser.

5.2.1.1.2. SURFACE TENSION GRADIENTS

As mentioned by [44], during laser surface melting, temperature gradients on the melt surface between the laser beam impact point and the intersection line of the solid-liquid interface with the surface lead to surface tension gradients that sweep liquid away from the beam impact

point. The temperature gradient extends radially away from the center of the laser beam. Under the laser beam, the temperature of the liquid is at the highest and surface tension of the liquid is at the lowest. As the liquid temperature decreases away from the center of the beam, the surface tension of the liquid increases. This phenomenon causes the liquid to flow away from the center of the beam and therefore depress the liquid surface underneath the laser beam and ridge the liquid surface elsewhere. As the beam passes to other areas of the surface, the height difference between the liquid under the beam and the liquid away from the beam increases. A pressure head induces a counter flow of liquid back to the region underneath the beam. At steady state, the liquid flow away from the beam caused by the surface tension gradient and the gravity counter flow of the liquid towards the beam balance each other out. Due to the large temperature gradients and rapid solidification rates associated with laser surface melting, this distortion of the liquid surface becomes frozen into the surface and ripples appear. The only manner in which these ripples from surface-tension gradients can be avoided is if the laser-beam sweep velocity exceeds a certain critical velocity. The following equation states the critical velocity that the laser beam must exceed [44]:

$$V_c = \frac{1}{2} h / \tau \quad \text{Eq. 5-1}$$

Where h is the ripple base width, τ is the time required to form ripples. Noting that the equation for τ is [44]:

$$\tau = (3h / g)^{1/2} \quad \text{Eq. 5-2}$$

Where, g is the acceleration field, V_c can be written as [44]:

$$V_c = (hg/12)^{1/2}$$

Eq. 5-3

However, a higher beam velocity requires a higher power laser in order to achieve the same penetration depth. The high power laser leads to additional cost and also surface rippling through other mechanisms such as vapour-pressure depression of the melt surface.

The surface tension, σ , of a liquid may be written as $\sigma = \sigma_0 - ST$. Here, σ_0 is the surface enthalpy, S is the surface entropy and T is the temperature. Since the surface entropy S is positive, the temperature coefficient $d\sigma/dT$ of the surface tension of most liquids is negative ($d\sigma/dT < 0$).

Figure 5-2 represents the various stages of the laser beam sweep and the creation of ripples due to surface tension gradients.

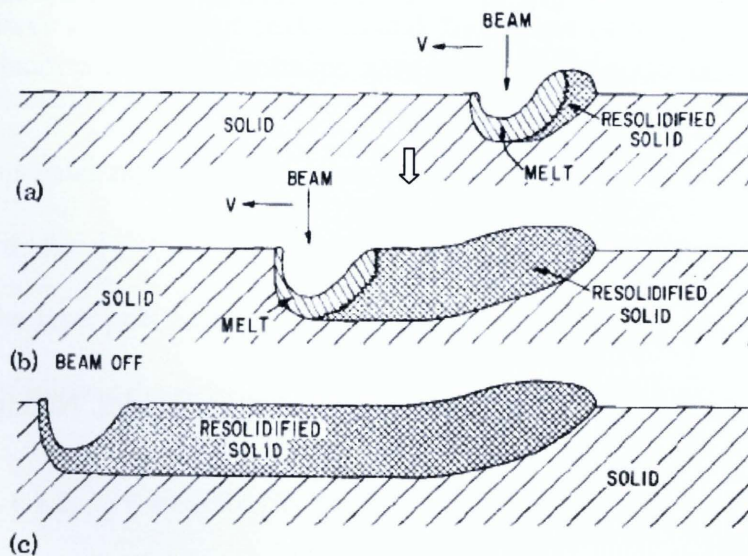


Figure 5-2: A midpoint cross section parallel to the laser beam path of a laser-melted surface illustrating rippling and key-holing effects. (a) Just after initiation of the laser beam sweep; (b) rippling and keyholing in steady state; (c) at the conclusion of the laser beam sweep [44]

5.2.1.1.3. INTERFERENCE BETWEEN THE INCIDENT LIGHT AND THE SURFACE WAVE

As [7] observes, the application of a moderate number ($N \approx 5$) of laser pulses creates the periodic surface structures called ripples. The authors state that these formations are not seen for single-pulse experiments and therefore a form of feedback mechanism is involved in the formation of the surface patterns. Ripples occur when solid surfaces are exposed to multiple subsequent pulses [45]. With increasing number of shots, the threshold for formation of ripples decreases significantly [45]. They appear as lines orthogonal to the direction of the electric field vector of the incident light and the period dependent on the wavelength of the generating light, the surface roughness and morphology of the surface [46, 47]. The main reasoning behind such structures is interference between the incident light and a surface wave which is generated by scattering [7, 45, 46]. The scattering is due to random variation in the height of the solid surface or poor crystalline quality of the surface layer or many other intrinsic and extrinsic factors [45]. That is, the fringes are caused by the optical interference of incoming light reflected from the surface and the back-reflected wave from the plasma, forming standing waves [46]. The interference causes periodic change in the absorbed intensity and therefore modulated ablation. The melting threshold is periodically exceeded and the rapid re-solidification of the thin molten layer gives rise to the ripples [45, 46]. These phenomena occur only when the laser intensity is high enough so that the surface temperature is close to the melting temperature [45, 46].

As [45] illustrates, the growth of the ripples is partially dependent on the surface temperature and whether the absorbed power is in phase or out of phase with the surface temperature variation. If the absorbed power is in phase, then the regions of higher initial

temperature will have a faster rate of temperature increase as a result of laser illumination. Therefore, the index variation also increases, the diffraction is stronger and the intensity fringes are more pronounced and ripple growth occurs. If the absorbed power is out of phase, then the power will be absorbed by regions that were initially colder and as a result no growth will occur. The authors also conclude that the growth coefficient (and to a smaller extent the actual spacing Λ) is based upon the actual value of the complex dielectric function. The growth is much faster if the material is metallic-like, that is, the relative permittivity (ϵ_r) is less than zero. Therefore, melting of the semiconductor is necessary.

According to [46], the first pulse causes random surface roughening; meanwhile, the subsequent pulses create periodic ripples that can be classified into S_+ , S_- or c fringes. The period of these ripples is dictated by the wavelength, polarization and incident angle of the laser. The S_+ and S_- type of ripples are perpendicular to the polarization and have a period of [45, 46]:

$$\Lambda_{\pm} = \lambda / (1 \pm \sin \theta) \quad \text{Eq. 5-4}$$

Where, θ is the angle of incidence. The S_- is usually dominant. The c type fringes are rarely formed and run parallel to the polarization and have a period of [46]:

$$\Lambda_c = \lambda / \cos \theta \quad \text{Eq. 5-5}$$

Thus, the spatial period Λ of these ripples is known to be closely related to the wavelength λ and angle of incidence [46].

5.2.1.1.4. BOSON CONDENSATION HYPOTHESIS

Others, [45, 48, 49], have suggested that surface plasmons produce the ripples. They charge that, when using ultrafast femtosecond lasers, mechanical and thermal forces do not have any effect because those forces associated with heat flow or material viscosity are immaterial over the distances of the order of wavelength or the absorption depth which are typically microns. These researchers proposed that the ripples were caused by the condensation of plasmons in very high carrier-density regions. In other words, the excitations are electronic in nature rather than thermal or mechanical. The so-called Boson Condensation Hypothesis can be reviewed in depth in [50]. In summary, Van Vechten proposed that the Boson Condensation requires a high carrier density ($>10^{23}$) on the anti-bonding state, for which plasmon energy is greater than the band gap energy of the material. Recent experiments show that when intense femtosecond pulses hit the material, a high carrier density is induced ($\geq 10^{23}$) in such a short time that the lattice remains cool. For such a density of carriers, the polarization waves begin to create and destroy electron-hole pairs in a coherent fashion so that they are no longer free independent carriers but rather paired carriers. These paired carriers behave as bosons, which condense in accordance with the BCS mechanism explained in [51]. Van Vechten suggests some tests to prove the hypothesis correct. For instance, Van Vechten said that if the hypothesis is true then a low intensity linearly polarized laser, hitting the substrate at the time the high reflectivity phase appears in the sample leads to linear ripples.

In the experiments conducted during this research, both femtosecond and picosecond laser pulse duration was used. In the femtosecond regime, the ripple formation on the silicon surface is based on the Boson Condensation Hypothesis since mechanical and thermal forces are

negligible, whereas in the picosecond regime, the ripple formation can be based on any or a combination of the other above-mentioned mechanisms.

5.2.1.2 EFFECT OF PULSE WIDTH ON RIPPLE SPACING

As [42] mentions, increase in the pulse width leads to increase in the ripple spacing. As shown in Table 5-1, the data supports such a conclusion. The effect is more pronounced for the higher laser repetition rate of 13 MHz compared to 8.67 MHz. This is due to the fact that, as the repetition rate increases, a larger number of pulses impact the silicon surface. Based on the data in Table 5-1, for 13 MHz, the ripple spacing is 0.48 μm at 300 fs compared to 1.06 μm at 5 ps. For 8.67 MHz, the ripple spacing remains almost constant. It varies from 0.44 μm at 300 fs to 0.43 μm at 5 ps. Refer to Figures 5-3 and 5-4 for sample SEM images of ripple formation. The ripple spacing has been marked on the pictures.

Laser Repetition Rate (MHz)	Pulse Width (femtoseconds)	Ripple Spacing (μm)
8.67	300	0.44
	700	0.42
	5000	0.43

13	300	0.48
	700	0.44
	5000	1.06

Table 5-1: Ripple Spacing vs. Pulse Width for Laser Repetition Rate of 8.67 and 13 MHz

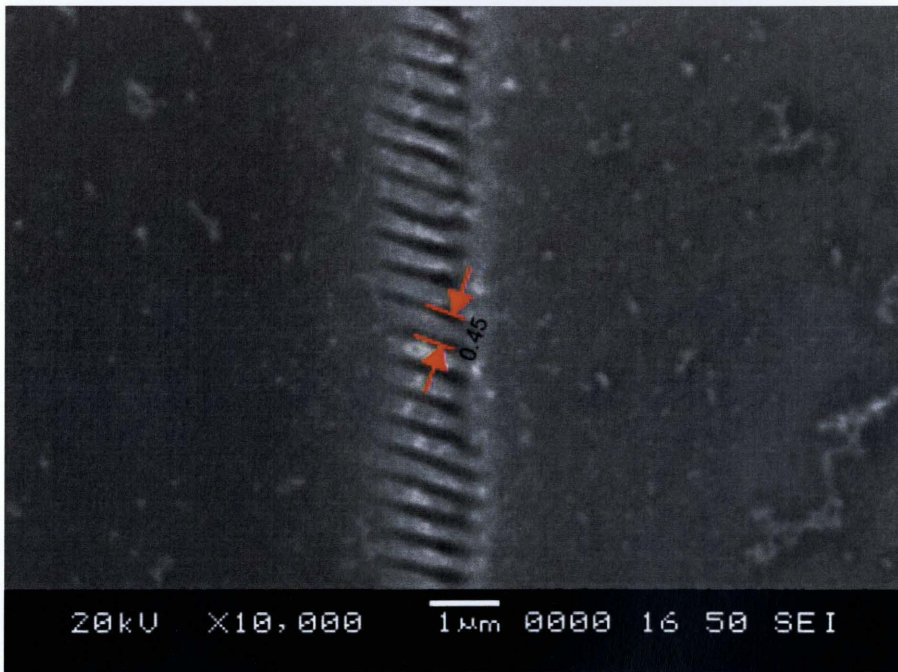


Figure 5-3: SEM image of ripple formation at 300 fs, 8.67 MHz laser repetition rate and 0.230 W laser power (equivalent to 2.653E-08 J pulse energy)

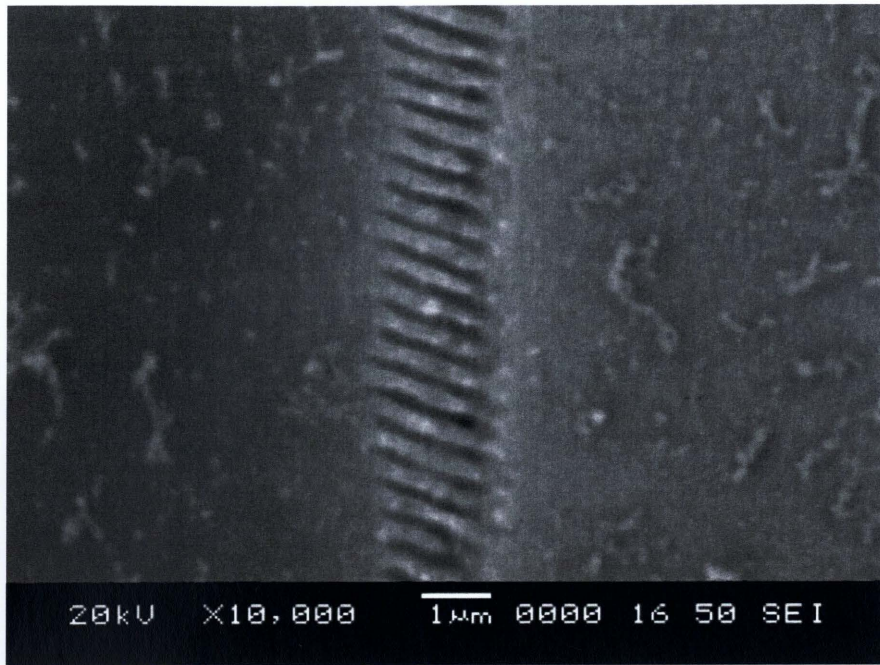


Figure 5-4: SEM image of ripple formation at 700 fs, 8.67 MHz laser repetition rate and 0.270 W laser power (equivalent to 3.114E-08 J pulse energy)

Considering the acoustic wave mechanism described before for generation of ripples and the analysis carried out in [52], Table 5-1 can be explained quite easily. First of all, d must be taken to be the full width ($d = 2a$) of the laser spot or line. Also, keep in mind that the gradient of the temperature is located at the origin of the sound generation. When d is large, the lateral gradient of the temperature profile is small, and hence the efficiency of the surface acoustic wave (SAW) is large as well. In the limit of a lateral infinite laser-pulse profile, only longitudinal waves are produced since there is only an axial gradient of the temperature due to thermal diffusion within the timescale of the laser pulse. When d is small, the efficiency is small as well because a point or very thin line source is obtained, the extent of which is small compared to the wavelengths produced. Therefore, there exists a certain diameter or width $2a$ of the laser pulse profile that allows for the most constructive interference of the individual SAW components

produced at each expanding surface element. From these arguments, maximal efficiency should occur if

$$d = 2\tau v_R \quad \text{Eq. 5-6}$$

holds. Here, v_R is the Rayleigh velocity and 2τ is the laser pulse width. Therefore, if the surface acoustic wave is deemed to be 3×10^3 m/s [42] for silicon and the frequency to be inverse of the laser pulse width (300 fs, 700 fs, 5 ps), a propagation distance during that time of 9×10^{-10} m, 2.1×10^{-9} m, 1.5×10^{-8} m is calculated, respectively, based on Equation 5-6. Although the values disagree with the experimental results, the overall trend is an increase in the pulse width leading to increase in the ripple spacing.

In quantitative terms, the findings can be described through two theoretical considerations relevant to the problem [52, 53]. In both, the radiant power is assumed to be modulated at a single frequency $\omega/2\pi$, whereas the lateral, spatial profile of the radiating beam is assumed to be rectangular of width d or Gaussian of full-width $2a$, corresponding to the experimental situation in this study. In the first case, maximal efficiency should occur if $k_R = \pi/2d$, and, in second case, for $k_R = \sqrt{2}/a = \sqrt{8}/d$. Here, k_R is the wave vector of the SAW. It is reassuring that both calculations give quite similar results. However, the spectrum of SAWs was generated due to the finite optical width. This can be incorporated into the theory presented by Krylov and Pavlov [53] in an easy manner. These authors calculated the potentials ϕ and ψ of the SAW which contained the Fourier transform $G(k)$ of the lateral shape of the laser pulse as a prefactor. The laser beam was assumed to be 100% modulated and focused perpendicular to the propagation direction. The potentials have the form [54]:

$$\Phi = BF(k_R)G(k_R)\exp(ik_Rx - qz) \quad \text{Eq. 5-7}$$

$$\Psi = BH(k_R)G(k_R)\exp(ik_Rx - sz) \quad \text{Eq. 5-8}$$

B contains the relevant thermal and optical parameters such as thermal expansion, optical reflectivity, optical absorption coefficient, bulk modulus, specific heat and density.

$q = (k_R^2 - k_l^2)^{1/2}$ and $s = (k_R^2 - k_t^2)^{1/2}$, where k_l and k_t are the wave vectors for longitudinal and transverse waves, respectively. The definition of $F(k_R)$ and $H(k_R)$ can be found in [53]. The propagation direction of the SAW is the x direction on an isotropic solid occupying the half-space $z \geq 0$.

As [54] points out, since the amplitude and the total intensity of the SAW is directly proportional to the prefactors squared of Φ and Ψ , the maximal efficiency can be calculated easily from equations (5-7) and (5-8). For a Gaussian intensity profile in the x direction, $I = I_0 \exp(-x^2/a^2)$, the Fourier transform is $G(k_R) = BH(a/\sqrt{\pi})\exp(-k_R^2 a^2/4)$ and therefore the maximum is obtained at $k_R = \sqrt{2}/a$. This means a first maximum at $k_R = \pi/2d$. Here, d is the width of a rectangular laser profile.

As described by [54], in the case of a circular laser spot, radial Rayleigh waves are generated which are not described by the potentials of equations (5-7) and (5-8). However, since the correct potentials will still contain the Fourier transform $G(k)$ of $I = I_0 \exp(-r^2/a^2)$ ($r = \sqrt{x^2 + y^2}$) as a prefactor, maximal efficiency is also obtained when $k_R = \sqrt{2}/a$. Moreover, equations (5-7) and (5-8) need to be multiplied by the Fourier transform of the temporal laser-pulse envelope due to the finite laser-pulse width. Assuming a Gaussian

shape $I = I_0 \exp(-t^2/\tau^2)$, another requirement arises in the form of maximal efficiency occurring only when $\omega_R = \sqrt{2}/\tau$ and since $\omega_R = v_R k_R$ to $k_R = \sqrt{2}/v_R \tau$. Equating the two conditions results in $a = v_R \tau$. After inserting, $v_R = a/\tau$ in $k_R = \sqrt{2}/v_R \tau$ we obtain $k_R = \sqrt{2}/a$.

5.2.1.3 EFFECT OF PULSE ENERGY ON RIPPLE SPACING

As [48] points out, with increasing power density or number of pulses, the spacing between the ripples increase. The data in this study does not point to any concrete relationship between ripple spacing and pulse energy. This is due to the fact that [48] used a 35 ps, 10 Hz and 1064 nm laser compared to the 5 ps, 13 MHz and 515 nm equipment used here. However, Figure 5-5 does further showcase the fact that the ripple spacing does increase with increase in the pulse width.

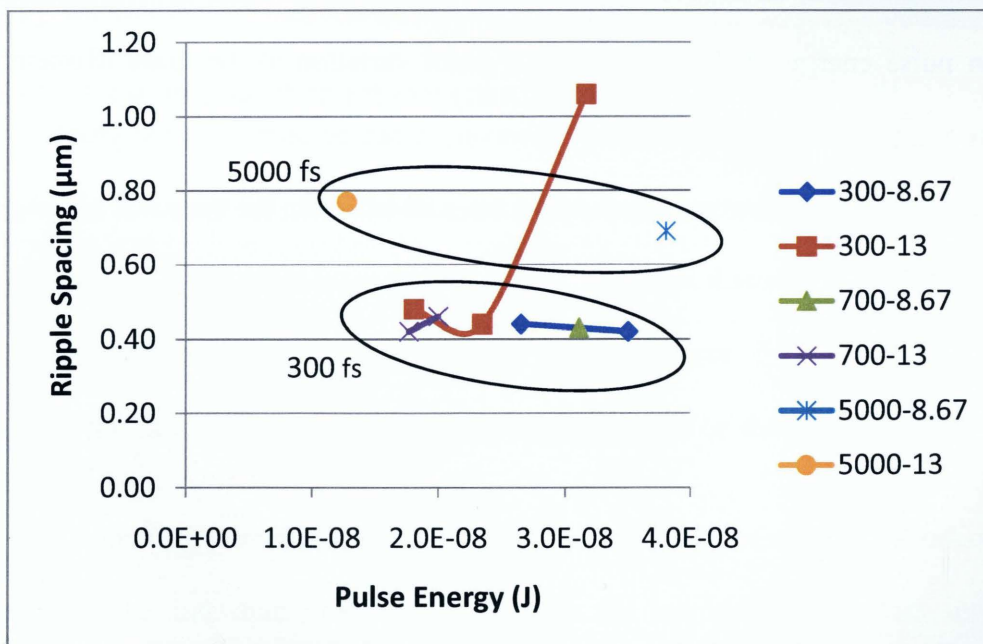


Figure 5-5: Ripple Spacing vs. Pulse Energy for Pulse Width 300 fs to 5 ps and Repetition Rate of 8.67 and 13 MHz

5.2.2 GRAINS

5.2.2.1 GRAIN FORMATION MECHANISM

As [48, 49] describe, irradiation with intense ultrashort laser pulses lead to bond weakening and breaking in the illuminated area of the semiconductor substrate. The ensuing rearrangement of the crystal lattice is short in duration and is in fact so fast that the compound effect of the short movements of defects and the creation of new bonds between the atoms leads to formation of grains. Because of the short pulse length the surface material heats up and cools down without the bulk material being involved. Therefore, the excitations are electronic excitations where the lattice remains cool.

5.2.2.2 EFFECT OF PULSE ENERGY ON GRAIN DIAMETER

From Figure 5-6, no conclusion can be made with regards to the dependence of grain diameter on pulse energy. Although there is a small variation in the grain diameter, it is too negligible to warrant further examination. However, it can be seen from the graph that the laser repetition rate (number of laser pulses) does not have an effect on the diameter of the grains.

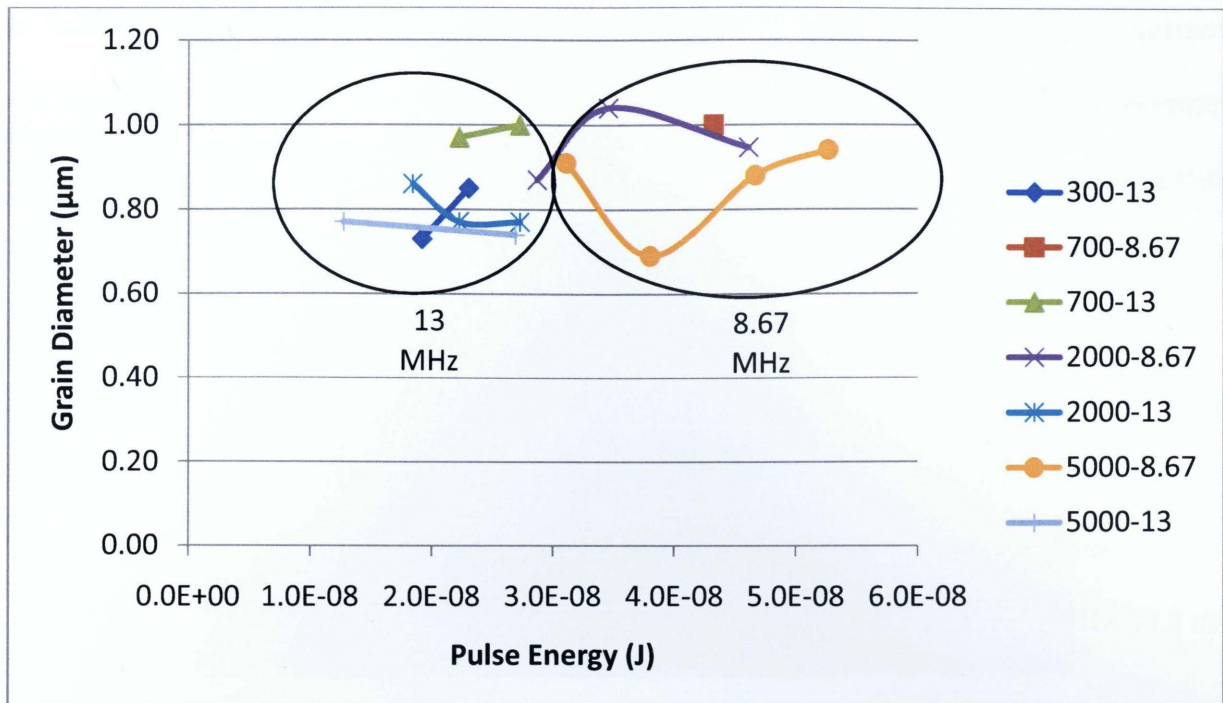


Figure 5-6: Grain Diameter vs. Pulse Energy for Pulse Width 300 fs to 5 ps and Repetition Rate of 8.67 and 13 MHz

5.2.2.3 EFFECT OF PULSE WIDTH ON GRAIN DIAMETER

As shown in Figure 5-7, for 13 MHz, the grain diameter changes from 0.73 μm at 300 fs to 1.00 μm at 5 ps. At 8.67 MHz laser repetition rate, the grain diameter varies from 1.00 μm at 700 fs to 1.14 μm at 2 ps back to 1.05 μm at 5 ps. Refer to Figures 5-8 and 5-9 for sample SEM images of grain formation. The grain diameter has been marked on the pictures.

As mentioned by [49], the natural movement or diffusion of atoms in semiconductors is possible through the introduction of defects. When the material temperature increases, the defects become very mobile. These defects accumulate to create extended absorption centers. This accumulation mechanism leads to growth of small structural defects, aggregation and

clustering of point defects and the formation of pits. The final morphology of the material is determined by the changes in the mobility of the defects and the relaxation processes after the redistribution of atoms in the crystal lattice. However, when femtosecond lasers are used, damage to semiconductor surfaces initiate without any pit formation. The damage occurs in the form of ablation. For multiple pulses, small pits do form, but are negligible in size compared to the pits formed in the picosecond regime. As a result, defects do not find sufficient time to move a large distance and form a large accumulation. Thus, the grain diameter is smaller in the femtosecond regime compared to the picosecond regime. Also, as the repetition rate is increased from 8.67 MHz to 13 MHz, the pulse energy reduces which leads to decrease in the grain sizes.

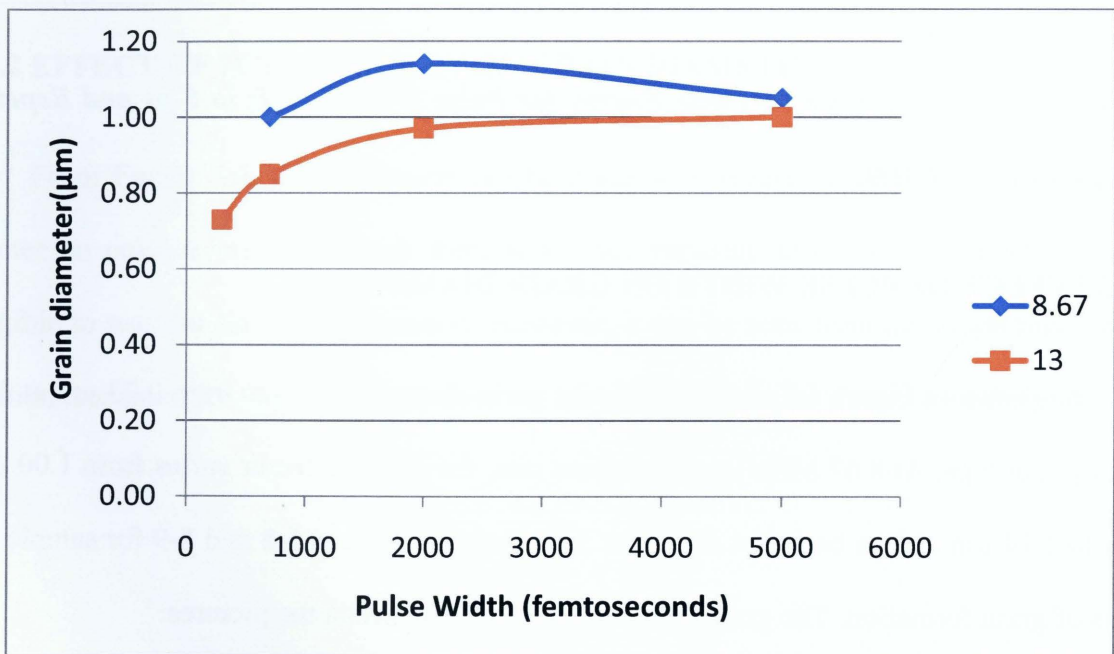


Figure 5-7: Grain Diameter vs. Pulse Width for Laser Repetition Rate of 8.67 and 13 MHz

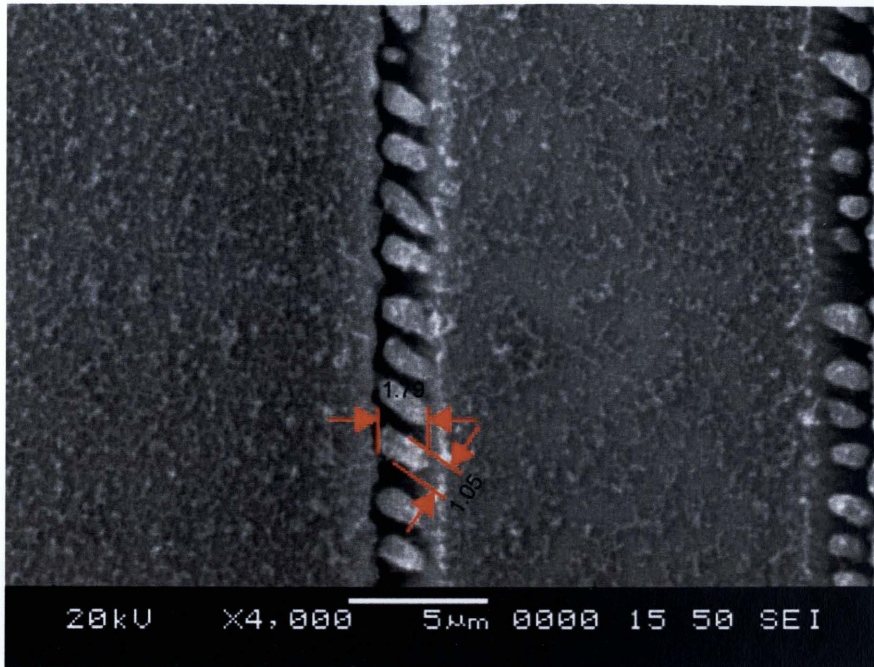


Figure 5-8: SEM image of grain formation at 700 fs, 13 MHz laser repetition rate and 0.320 W laser power (equivalent to 2.462E-08 J pulse energy)

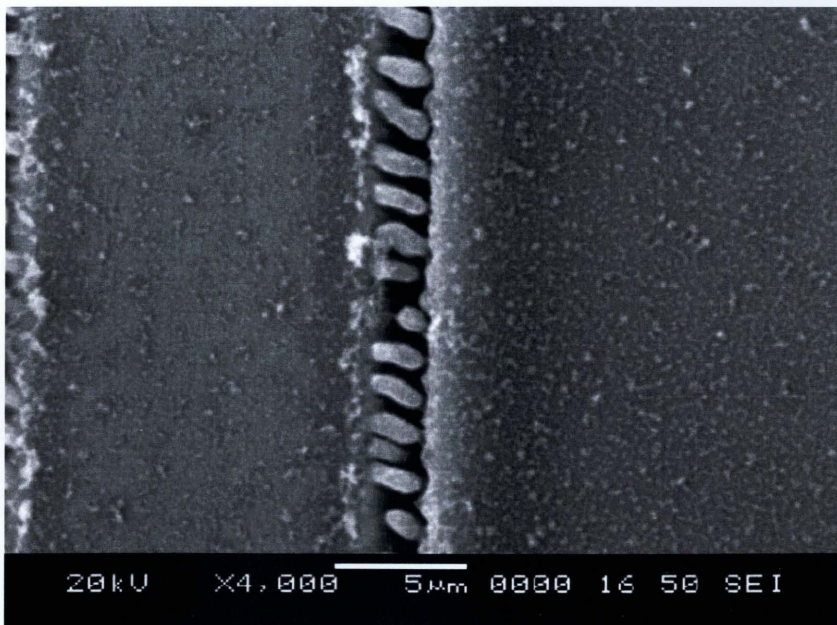


Figure 5-9: SEM image of grain formation at 2000 fs, 8.67 MHz laser repetition rate and 0.249 W laser power (equivalent to 2.872E-08 J pulse energy)

5.3 SUMMARY

Surface patterning using a femtosecond laser can be utilized for the fabrication of MEMS/NEMS, CMOS, 3D-microstructures, micro trenches, micro channels, micro holes, periodical submicron gratings and nanophotonics. A unique high repetition rate femtosecond fiber laser system was used to study the effect of pulse width, repetition rate and pulse energy on the spacing of ripples, as well as diameter of grains created during the surface patterning operations. In the experiments, the ripples formed at a lower laser fluence range of 1.56 J/cm^2 to 4.66 J/cm^2 , whereas the grains were created at a higher laser fluence range of 3.34 J/cm^2 to 6.77 J/cm^2 . The primary theory used to explain the creation of ripples in the femtosecond regime was the Boson Condensation Hypothesis since mechanical and thermal forces are deemed to be negligible. For the picosecond pulse width range, the ripple formation can be based on any or a combination of the acoustic wave, surface tension gradient and interference between the incident light/surface wave mechanisms. The grain formation in both the femtosecond and the picosecond span used in this research is due to the bond weakening and breaking in the silicon substrate and the short duration of the crystal lattice rearrangement following illumination by the laser. The small movements lead to the creation of new bonds between the atoms and eventual formation of grains. It was seen that, for the pulse width, repetition rate and pulse energy range used, the ripple spacing increased with laser pulse duration while other parameters did not play an important role. In terms of grain diameter, a similar trend was seen.

CHAPTER 6

SUMMARY, CONCLUSIONS AND FUTURE WORK

6.1 SUMMARY & CONCLUSIONS

The objective of this thesis was to propose, investigate and develop a femtosecond laser nanomachining technique that can overcome the challenges faced by the conventional techniques currently in use in different industries.

In this thesis, the currently used nanofabrication techniques such as DUV and Vacuum-UV lithography, EUV and X-ray Lithography, Electron Beam Lithography, Ion Beam Lithography and finally Femtosecond Laser Nanomachining were described. The femtosecond laser technique was identified to be the most capable technique for achieving the goals of high throughput, high quality, least thermal damage and least machining debris with the lowest cost.

Although the feasibility of using femtosecond lasers for nanomachining has been predicted for some time, industrial application of this technique has not been widespread due to the challenges faced in terms of laser parameters and inadequate experimental studies in this area. For precise material processing, thorough knowledge of the fundamental physics governing the interaction of laser radiation with matter is crucial. The physical processes of laser-matter interaction were successfully studied and also the mechanisms and phenomena involved in both the nanosecond and femtosecond laser regimes were explained.

For this study, a high repetition rate femtosecond laser system was chosen. An efficient and yet simple experimental setup was arrived at after studying the capabilities of the proposed laser system while keeping the objectives of the research in mind.

The experimental results outlined in Chapter 4 demonstrate that a high pulse repetition rate is ideal for nanomachining of thin films. It was seen that high repetition rates lead to smaller craters with uniform line width. Craters created at a 13 MHz pulse repetition rate with 2.042 J/cm² beam energy fluence measured 110 nm in width and had a heat affected zone of 0.79 μm. It was found that the pulse repetition rate did not play a significant role in the size of the heat affected zone for different laser fluences. However, higher laser energy fluence led to a larger heat affected zone.

The experimental results outlined in Chapter 5 demonstrate primarily the effect of laser pulse width on the spacing of ripples, as well as diameter of grains created during irradiation. In the experiments, the ripples formed at a laser fluence range of 1.56 J/cm² to 4.66 J/cm², while grains were created at a laser fluence range of 3.34 J/cm² to 6.77 J/cm². In the femtosecond regime, the ripple formation on the silicon surface was based on the Boson Condensation Hypothesis since mechanical and thermal forces are deemed to be negligible, whereas in the picosecond regime, the ripple formation can be based on any or a combination of the acoustic wave, surface tension gradient and interference between the incident light/surface wave mechanisms. The grain formation in both the femtosecond and the picosecond range is due to the bond weakening and breaking in the silicon substrate and the short duration of the crystal lattice rearrangement following illumination by the laser. The excitations that lead to the creation of these grains are electronic in nature. It was seen that, for the pulse width, repetition rate and

pulse energy range used in this thesis, the ripple spacing increased with laser pulse duration while other parameters did not play a crucial role. In terms of grain diameter, a similar trend was seen.

In conclusion several important contributions were made by this study as outlined:

- It was proven that a high repetition rate femtosecond laser system is ideal for nanomachining of silicon wafers. Craters were created at 13 MHz pulse repetition rate with 2.042 J/cm^2 beam energy fluence that measured 110 nm in width and had a heat affected zone of $0.79 \text{ }\mu\text{m}$.
- The influence of laser repetition rate and pulse energy on crater width and heat affected zone (HAZ) of silicon wafers during nanomachining above the ablation threshold was evaluated.
- The effect of the pulse width, repetition rate and pulse energy on the spacing of ripples as well as diameter of grains created on silicon wafers during nanomachining below the ablation threshold (surface patterning) was examined.

6.2 FUTURE WORK

The laser system used in these experiments does have shortcomings especially for the study carried out in Chapter 4. The laser used has a maximum average power of 12 W. The experiments used a power of less than 0.5 W. As a result, all of the results suffered from high power fluctuation as evident in the SEM images. The applications considered in this research would require a laser system with a lower maximum average power of approximately 1 W to obtain stable pulse energy leading to uniform line width. Such a system would be capable of

smaller pulse energy increments allowing for more precise control of feature size. Future research should utilize a 1 W laser system to repeat the study in Chapter 4 in order to further optimize the repetition rate that would create the minimal feature size with the least heat affected zone. Using this kind of setup, along with techniques such as radial polarization and a different gas assist, may enable the creation of sub 100 nm feature size with good quality. Enclosing the laser system would also help in this regard.

In the experiments outlined in this thesis, the second harmonic (515 nm) central wavelength was used. As a future work, these experiments can be performed at lower wavelengths by using third harmonics. Even with the loss of laser power associated with the frequency tripling, this kind of setup may be able to further improve the quality of the machining, as well as further reduce the size of the nano features on the silicon wafer.

REFERENCES

- [1] M. Kohler and W. Fritzsche, Nanotechnology: An Introduction to Nanostructuring Techniques, Weinheim, Germany: Wiley-VCH, 2nd Edition, 2007
- [2] Semiconductor Media Limited, London, UK, (March 29, 2009) <http://www.fabtech.org>
- [3] W. Kröninger and F. Mariani, "Thinning and Singulation of Silicon: Root Causes of the Damage in Thin Chips", 2006 Proceedings – 56th Electronic Components and Technology Conference, San Diego, CA, USA, 2006, pp. 1317-22
- [4] B.N. Chichkov, C. Momma, S. Nolte, F. Von Alvensleben and A. Tünnermann, "Femtosecond, Picosecond and Nanosecond Laser Ablation of Solids", Applied Physics A: Materials Science and Processing, Vol. 63, No. 2 (1997), pp. 109-15
- [5] P.P. Pronko, S.K. Dutta, J. Squier, J.V. Rudd, D. Du and G. Mourou, "Thermophysical Effects in Laser Processing of Materials with Picosecond and Femtosecond Pulses", Journal of Applied Physics, Vol. 78, No. 10 (1995), pp. 6233-40
- [6] E. G. Gamaly, A.V. Rode and B. Luther-Davies, "Ultrafast Ablation with High-Pulse-Rate Lasers. Part I: Theoretical Considerations", Journal of Applied Physics, Vol. 85, No. 8 (1999), pp. 4213-21
- [7] J. Bonse, S. Baudach, J. Krüger, W. Kautek and M. Lenzner, "Femtosecond Laser Ablation of Silicon: Modification Thresholds and Morphology", Applied Physics A: Materials Science and Processing, Vol. 74, No. 1 (2002), pp. 19-25
- [8] C. Schäfer, H. M. Urbassek and L.V. Zhigilei, "Metal Ablation by Picosecond Laser Pulses: A Hybrid Simulation", Physical Review B: Condensed Matter and Materials Physics, Vol. 66, No. 11 (2002), pp. 115404/1-8

- [9] P. Lorazo, L.J. Lewis and M. Meunier, "Short-Pulse Laser Ablation of Solids: From Phase Explosion to Fragmentation", Physical Review Letters, Vol. 91, No. 22 (2003), pp. 225502/1-4
- [10] B. Pecholt, M. Vendan, Y. Dong and P. Molian, "Ultrafast Laser Micromachining of 3C-SiC thin films for MEMS Device Fabrication", International Journal of Manufacturing Technology, Vol. 39 (2007), pp. 239-50
- [11] L. Curran, "Diamond Scribes Start to Give Way to Laser Machines, Slurry Saws, New Etch Methods", Electronics, Vol. 43, No. 24 (1970), pp. 70-5
- [12] D. Perrottet, K. Dunne, G. Walsh and B. Diggin, "Using Lasers to Dice Thin Silicon Wafers", Advanced Packaging, Vol. 17, No. 3 (2008), pp. 35-36+42
- [13] J. Vittu, D. Perrottet, J.M. Buchilly and B. Richerzhagen, "Damage-Free Dicing of Low-K Wafers", Future FAB International
- [14] M. Schmidt and G. Eßer, "The Future of Lasers in Electronics", ICALEO 2003 - 22nd International Congress on Applications of Laser and Electro-Optics, Congress Proceedings, Jacksonville, FL, USA, 2003
- [15] G.A. Hardway, "Applications of Laser Systems to Microelectronics and Silicon Wafer Dicing", Solid State Technology, Vol. 13, No. 4 (1970), pp. 63-7
- [16] Al A. Kolomenskii, H.A. Schuessler, V.G. Mikhalevich and A.A. Maznev, "Interaction of Laser-Generated Surface Acoustic Pulses with Fine Particles: Surface Cleaning and Adhesion Studies", Journal of Applied Physics, Vol. 84, No. 5 (1998), pp. 2404-10
- [17] M. Henry, J. Wendland and P.M. Harrison, "Nanoscale Analysis of Laser Ablated Thin Films used in Industrial Manufacturing of Flat Panel Displays", ICALEO 2006 - 25th International Congress on Applications of Laser and Electro-Optics, Congress Proceedings, Scottsdale, AZ, 2006

- [18] P. Leidere, J. Boneberg, V. Dobler, M. Mosbacher, H.J. Muenzer, N. Chaoui, J. Siegel, J. Solis, C.N. Afonso, T. Fourrier, G. Schrems and D. Baeuerle, "Laser-Induced Particle Removal from Silicon Wafers", Proceedings of SPIE - The International Society for Optical Engineering, Vol. 4065, Santa Fe, NM, USA, 2000, pp. 249-59
- [19] Clark-MXR Inc., Dexter, MI, USA, (Feb. 4, 2008)
<http://www.cmxr.com/Industrial/Handbook>
- [20] J. Yi-Jie Jia, "The Mechanism of Thin Film Si Nanomachining Using Femtosecond Laser Pulses", Master of Science Thesis, June 2004, Massachusetts Institute of Technology (MIT)
- [21] L. Shah, A.Y. Arai, S.M. Eaton and P.R. Herman, "Waveguide writing in fused silica with a femtosecond fiber laser at 522 nm and 1 MHz repetition rate", Optics Express, Vol. 13, No. 6 (2005), pp. 1999-2006
- [22] Physik Instrumente (PI) GmbH & Co. KG, Karlsruhe/Palmbach, Germany, (Mar. 15, 2008)
<http://www.physikinstrumente.com/en/products/prdetail.php?sortnr=300710>
- [23] Special Optics, Wharton, NJ, USA, (Mar. 15, 2008)
<http://www.specialoptics.com/Telecentric%20UV%20Scanning%20Lenses.html>
- [24] Y. Dong and P. Molian, "Femtosecond pulsed laser ablation of 3C-SiC thin film on silicon", Applied Physics A: Materials Science Processing, Vol. 77, No. 6 (2003), pp. 839-46
- [25] K. Venkatakrishnan, B. Tan and B.K.A. Ngoi, "Femtosecond pulsed laser ablation of thin gold film", Optics & Laser Technology, Vol. 34 (2002), pp. 199-202
- [26] J. Kim and S. Na, "Metal thin film ablation with femtosecond pulsed laser", Optics & Laser Technology, Vol. 39 (2007), pp. 1443-48

- [27] R. Haight, A. Wagner, P. Longo and D. Lim, "Femtosecond laser ablation and deposition of metal films on transparent substrates with applications in photomask repair", Proceedings of SPIE - The International Society for Optical Engineering, Vol. 5714, San Jose, CA, USA, 2005, Commercial and Biomedical Applications of Ultrafast Lasers V, 2005, pp. 24-36
- [28] K. Mukaihara, M. Yoshioka, S. Ito and Y. Suzuki, "351 nm femtosecond laser with Nd:glass regenerative amplifier for thin films ablation", Proceedings of SPIE - The International Society for Optical Engineering, Vol. 6108, San Jose, CA, USA, 2006, Commercial and Biomedical Applications of Ultrafast Lasers VI, 2006, pp. 206-13
- [29] S. Zoppel, H. Huber and G.A. Reider, "Selective ablation of thin Mo and TCO films with femtosecond laser pulses for structuring thin film solar cells", Applied Physics A: Materials Science & Processing, Vol. 89, No. 1 (2007), pp. 161-3
- [30] D. Ruthe, K. Zimmer and T. Höche, "Etching of CuInSe₂ thin films-comparison of femtosecond and picosecond laser ablation", Applied Surface Science, Vol. 247, No. 1-4 (2005), pp. 447-52
- [31] K. Venkatakrishnan, P. Stanley and L.E.N. Lim, "Femtosecond laser ablation of thin films for the fabrication of binary photomasks", Journal of Micromechanics and Microengineering, Vol. 12 (2002), pp. 775-79
- [32] K. Venkatakrishnan, B. Tan and N.R. Sivakumar, "Sub-micron ablation of metallic thin film by femtosecond pulse laser", Optics & Laser Technology, Vol. 34 (2002), pp. 575-8
- [33] K. Venkatakrishnan, P. Stanley, N.R. Sivakumar, B. Tan and L.E.N. Lim, "Effect of scanning resolution and fluence fluctuation on femtosecond laser ablation of thin films", Applied Physics A: Materials Science and Processing, Vol. 77, No. 5 (2003), pp. 655-58

- [34] A. Borowiec and H.K. Haugen, "Femtosecond laser micromachining of grooves in indium phosphide", Applied Physics A: Materials Science Processing, Vol. A79, No. 3 (2004), pp. 521-29
- [35] S.M. Eaton, H. Zhang, P.R. Herman, F. Yoshino, L. Shah, J. Bovatsek and A.Y. Arai, "Heat accumulation effects in femtosecond laser-written waveguides with variable repetition rate", Optics Express, Vol. 13, No. 12 (2005), pp. 4708-16
- [36] R.R. Gattass, L.R. Cerami and E. Mazur, "Micromachining of bulk glass with bursts of femtosecond laser pulses at variable repetition rates", Optics Express, Vol. 14, No. 12 (2006), pp. 5279-84
- [37] R. Böhme, K. Zimmer and B. Rauschenbach, "Direct laser etching of transparent materials: High quality surface patterning and figuring for micro-optical applications", Proceedings of SPIE - The International Society for Optical Engineering, Vol. 6254, Chernivtsi, Ukraine, 2005, Seventh International Conference on Correlation Optics, 2005, pp. 1-9
- [38] S. Chen, V.V. Kancharla and Y. Lu, "Laser-based microscale patterning of biodegradable polymers", International Journal of Materials & Product Technology, Vol. 18, No. 4-6 (2003), pp. 457-68
- [39] C.S. Lim, M.H. Hong, Y. Lin, G.X. Chen, A.S. Kumar, M. Rahman, L.S. Tan, J.Y.H. Fuh and G.C. Lim, "Sub-micron surface patterning by laser irradiation through microlens arrays", Journal of Materials Processing Technology, Vol. 192-193, No. 1-7 (2007), pp. 328-33
- [40] K. Katayama, H. Yonekubo and T. Sawada, "Formation of ring patterns surrounded by ripples by single-shot laser irradiation with ultrashort pulse width at the solid/liquid interface", Applied Physics Letters, Vol. 82, No. 24 (2003), pp. 4244-6
- [41] P.L. Liu, R.Yen, N. Bloembergen and R.T. Hodgson, "Picosecond laser-induced melting and resolidification morphology on Si", Applied Physics Letters, Vol. 34, No. 12 (1979), pp. 864-6

- [42] D. Jost, W. Luthy, H.P. Weber and R.P. Salathe, "Laser pulse width dependent surface ripples on silicon", Applied Physics Letters, Vol. 49, No. 11 (1986), pp. 625-7
- [43] G. Gorodetsky, J. Kanicki, T. Kazyaka and R.L. Melcher, "Far UV Laser Melting of Silicon", Applied Physics Letters, Vol. 46, No. 6 (1985), pp. 547-9
- [44] T.R. Anthony and H.E. Cline, "Surface rippling induced by surface-tension gradients during laser surface melting and alloying", Journal of Applied Physics, Vol. 48, No. 9 (1977), pp. 3888-94
- [45] Z. Guosheng, P.M. Fauchet and A.E. Siegman, "Growth of spontaneous periodic surface structures on solid during laser illumination", Physical Review B, Vol. 26, No. 10 (1982), pp. 5366-81
- [46] A.M. Ozkan, A.P. Malshe, T.A. Railkar, W.D. Brown, M.D. Shirk and P.A. Molian, "Femtosecond Laser Induced Periodic Structure Writing on Diamond Crystals and Microclusters", Applied Physics Letters, Vol. 75, No. 23 (1999), pp. 3716-18
- [47] N. Yasumaru, K. Miyazaki and J. Kiuchi, "Fluence dependence of femtosecond-laser-induced nanostructure formed on TiN and CrN", Applied Physics A: Materials Science & Processing, Vol. 81, No. 5 (2005), pp. 933-7
- [48] A.P. Singh, A. Kapoor, K.N. Tripathi and G. Ravindra Kumar, "Laser damage studies of silicon surfaces using ultra-short laser pulses", Optics and Laser Technology, Vol. 34 No.1 (2002), pp. 37-43
- [49] A.P. Singh, A. Kapoor and K.N. Tripathi, "Ripples and grain formation in GaAs surfaces exposed to ultrashort laser pulses", Optics and Laser Technology, Vol. 34, No. 7 (2002), pp. 533-40
- [50] J.A. Van Vechten, "Experimental tests for boson condensation and superconductivity in semiconductors during pulsed beam annealing", Solid State Communications, Vol. 39, No. 12 (1981), pp. 1285-91
- [51] J. Bardeen, L.N. Cooper and J.R. Schrieffer, Phys. Rev. 108, 1175 (1957); J. R. Schrieffer, "Theory of Superconductivity" (Benjamin, New York, 1964)

- [52] W. Arnold, B. Betz and B. Hoffmann, "Surface-Acoustic-Wave Generation by Thermoelasticity [and Discussion]", Rayleigh-Wave Theory and Application: Proceedings of an International Symposium, 1985, pp. 119-21
- [53] V.V. Krylov and V.I. Pavlov, "Thermo-optical generation of surface acoustic waves in a solid", Soviet Physics: Acoustics, Vol. 28, No. 6 (1982), pp. 493-4
- [54] W. Arnold, B. Betz and B. Hoffmann, "Efficient generation of surface acoustic waves by thermoelasticity", Applied Physics Letters, Vol. 47, No. 7 (1985), pp. 672-4